NTNU
Innovation and Creativity

Theory, Simulation and Measurement of Wireless Multipath Fading Channels

Kristian Mella

Master of Science in Communication Technology
Submission date: May 2007
Supervisor: Terje Røste, IET

Norwegian University of Science and Technology
Department of Electronics and Telecommunications

Problem Description

These thesis focus on the features of the wireless channel of the 2GHz band, aiming the WiMAX standard.
Relevant channel-theory should be covered, such as empirical channel models and types of fading. The thesis cover Matlab simulations of multipath fading channels based on a chosen model. WiMAX capacity estimations are performed in Matlab for a selected channel model. By means channel measurement equipment borrowed from Telenor R&D, practical measurements of multipath channels are performed.

Assignment given: 22. January 2007
Supervisor: Terje Røste, IET

Theory, Simulation and Measurement of Wireless Multipath Fading Channels

Kristian Mella

May 23, 2007

Contents

1 Introduction **1**

1.1 Objective 1

1.2 Background 1

1.3 Scope 2

2 Theoretical Aspects **4**

2.1 Free Space Path Loss 4

2.2 Path Loss Models 5

2.2.1 Introduction to Path Loss Models 5

2.2.2 Standards for Empirical Path Loss 6

2.2.3 Comments on Path Loss Models 10

2.3 Channel Metrics 10

2.3.1 Delay Profile and Delay Spread 10

2.3.2 Doppler Spread and Coherence Time 12

2.4 Signal Fading 13

2.4.1 Shadowing 13

2.4.2 Multipath Effects 14

2.4.3 Doppler Fading Effects 16

2.4.4 Small-Scale Fading Models 18

3 Matlab Simulations **21**
3.1 Introduction . . . 21
3.2 Simulation of Multipath Channel Measurement . . . 22
3.2.1 The Chirp Signal . . . 22
3.2.2 System Overview . . . 24
3.2.3 Implementation . . . 28
3.2.4 Simulation Results . . . 35
3.3 Capacity Simulations . . . 45
3.3.1 Introduction and Parameter Settings . . . 45
3.3.2 Implementation . . . 45
3.3.3 Results and Analysis . . . 48

4 Channel Measurements **56**
4.1 Objective and Scope . . . 56
4.2 Equipment . . . 57
4.2.1 Brief Overview . . . 57
4.2.2 Hardware . . . 57
4.2.3 Software . . . 60
4.3 Process . . . 62
4.4 Results and Analysis . . . 64

5 Conclusion **66**

6 Acronyms **68**

A Code Appendix **70**
A.1 Simulation Code . . . 70
A.1.1 measurement_simulation.m . . . 70
A.1.2 capacity_simulation.m . . . 75
A.2 Base Code . . . 82
A.2.1 global_variables_initialize.m . . . 82
A.2.2 chirp_signal_generation.m . . . 83
A.2.3 chirp_signal_generation_inverse.m . . . 84
A.2.4 channel_filter_cascade.m . . . 84

A.2.5 cos_roll_off.m 87
A.2.6 doppler_filter.m 87
A.2.7 gaussian_doppler_filter.m 89
A.2.8 generate_noise.m 90
A.2.9 OFDM_get_subcarriers.m 91
A.3 Channel Measurement Data Acquisition Code 92
A.3.1 ReadMeas.m 92
A.3.2 TIMEproc.m 95

B Figure Appendix **97**
B.0.3 Channel Measurements: Receiver Rack 97
B.0.4 Channel Measurements: Transmitter Rack 98

Bibliography **99**

List of Figures

2.1 Okumura Model: Median attenuation relative to free space over quasi-smooth terrain 7

2.2 Okumura Model: G_{area} correction factors for different terrains 7

2.3 Values of the SUI Model constants a, b and c 10

2.4 Multipath channel impulse response 11

2.5 Multipath power delay profile 12

2.6 Typical Doppler scenario 12

2.7 Doppler spectrum. f_c = carrier frequency, and f_m =maximum Doppler frequency 13

2.8 Typical path loss behaviours: (a) Average path loss from an empirical model (b) including effects from shadowing (c) superimposed by multipath fading 15

2.9 Two-ray ground reflection scenario 16

2.10 The manifestations of fading channels 17

2.11 Link budget considerations for fading channels 18

2.12 Rayleigh PDF 19

3.1 Chirp System. The impulse response of the chirp system is a chirp signal 22

3.2 Plot of Time Domain Chirp and its Autocorrelation Function 23

3.3 Plot of the LFM Chirp Frequency Response 23

3.4 Transmitter - Receiver Chain for Channel Measurements . . . 25

3.5 Frequency Response of LFM Chirp at $F_s = 100MHz$, real part 25

3.6 System Model of Multipath Rayleigh Fading 27

3.7 Raised Cosine System Filter. One-sided BW is 30MHz and roll-off factor α is 0.5 30
3.8 Cascade of System Filter and Channel given 4 Paths 31
3.9 Multipath Channel given 4 Paths 31
3.10 Doppler Filtering Process and Fading Coefficients. Mobile Communication. 32
3.11 Gaussian Doppler Filtering Process and Fading Coefficients. Fixed Communication. 32
3.12 Real Part of Generated Noise Samples ($\sigma_{noise} = 0.1$ and zero mean) 33
3.13 System Output: Measured Channel Profile versus Time (Mobile Simulation) 35
3.14 System Output: Measured Channel Profile versus Time, Rotated version of Figure 3.13 (Mobile Simulation) 39
3.15 System Output: Measured Channel Profile of the first chirp. The bottom plot is zoomed for illustration purposes (Mobile Simulation) 39
3.16 Generated Multipath Channel, 6 paths before fading (Mobile Simulation) 40
3.17 Cascade of the Multipath Channel and System Filter, 6 paths before fading (Mobile Simulation) 40
3.18 Doppler Filter, Gauss Samples and Doppler Filtered Samples for the First Tap (Mobile Simulation) 41
3.19 Same as Figure 3.18, but the lower plot is zoomed in on the 150 first samples for comparison with Figure 3.13 (Mobile Simulation) 41
3.20 System Output: Measured Channel Profile versus Time (Fixed Simulation) 42
3.21 System Output: Measured Channel Profile versus Time, Rotated version of Figure 3.20 (Fixed Simulation) 42
3.22 System Output: Measured Channel Profile of the first chirp. The bottom plot is zoomed for illustration purposes (Fixed Simulation) 42
3.23 Generated Multipath Channel, 6 paths before fading (Fixed Simulation) 43
3.24 Cascade of the Multipath Channel and System Filter, 6 paths before fading (Fixed Simulation) 43

3.25 Gaussian Doppler filter, Gauss samples and filtered samples for the first tap (Fixed Simulation) 44
3.26 Same as Figure 3.25, but the lower plot is zoomed in on the 500 first samples for comparison with Figure 3.20 (Fixed Simulation) 44
3.27 Flat AWGN channel: system response, transmitted OFDM symbol, system response over OFDM bandwidth 48
3.28 Flat AWGN channel: Maximum and Minimum received SNR levels over OFDM bandwidth 49
3.29 Fixed Communication Capacity Simulation: system response for 4 paths, OFDM symbol and response over OFDM symbol bandwidth 50
3.30 Received signal levels over the OFDM bandwidth at maximum and minimum capacity (Fixed) 50
3.31 Capacity CDF (Fixed) 51
3.32 Capacity PDF (Fixed) 51
3.33 Capacity PDF after reducing Transmitter Gain from 12dB to 6.5dB (Fixed) 52
3.34 Capacity CDF (Mobile) 53
3.35 Capacity PDF (Mobile) 53
3.36 Capacity PDF after reducing Transmitter Gain from 12dB to 6dB (Mobile) 54
3.37 Received signal levels over the OFDM bandwidth at maximum and minimum capacity (Mobile) 54
3.38 Mobile Communication Capacity Simulation: system response for 4 paths, OFDM symbol and response over OFDM symbol bandwidth 55

4.1 Channel Sounder Transmitter Hardware 58
4.2 Channel Sounder Receiver Hardware 59
4.3 Channel Sounder Software Overview 61
4.4 Arrangement of Receiver and Transmitter for the 2 indoor channel measurements performed 63
4.5 Plot of measured channel impulse response of first measurement at t=50s, as a product of averaging of 16 consecutive chirps 64

B.1 Receiver Equipment 97
B.2 Transmitter Equipment 98

Abstract

Multipath fading is a very common phenomenon in signal transmission over wireless channels. When a signal is transmitted over multipath channels, it is subject to reflection, diffraction and refraction. This results in multiple versions of the same signal to arrive at the receiver, each of which has suffered from various path loss, time-delay, phase shift and often also frequency shift. The latter is a result of Doppler shifts, which is experienced whenever a relative movement between the receiver and transmitter or scatterers is present. The communication environment changes quickly over location or time, thus introducing uncertainties to the channel response. Such channels result in increased system complexity, and the propagation effects need to be identified in order to predict the channel behaviour. Path loss is experienced in all types of radio channels, and its metrics are often determined by empirical path loss models. The path loss effects the mean received signal level, whereas large-scale fading (Shadowing) results in large-scale fluctuations of this received level. These variations are superimposed by the small-scale fluctuations, or small-scale fading, caused by multipath reception and Doppler shifts. Small-scale fading is simulated to gain a better understanding of these effects. In order to observe these effects satisfactory, the whole digital radio communication system chain must be simulated. Simulations are also performed for estimating the data capacity over both mobile and fixed multipath channels, and the resulting capacity of multipath reception exceeds the capacity of a flat channel due to increased received energy. In order to classify the effect of multipath channels on signal transmission, the profile of the channel for a given scenario has to be known, i.e. channel metrics such as the RMS delay spread is essential for a successful radio system design. A multipath channel profile and its RMS delay spread can be derived from a vast number of channel measurements performed for a given scenario. Measurements on the multipath channel impulse response have been performed, RMS delay spread has been calculated, and the procedure of the channel measurement process itself is simulated in Matlab.

Chapter 1

Introduction

1.1 Objective

This report is a product of the final thesis carried out at the Norwegian University of Science and Technology 2007. The objective is to quantify general propagation effects of both fixed and mobile wireless channels, with focus on multipath effects, and to simulate and measure multipath fading channels. The theoretical aspects should investigate relevant metrics for multipath channels, and serve as a basis of information for comprehension of the simulations and measurements.

The Matlab simulations should comprise realizations of the elements of a digital communication system chain, for correct estimation of a practical scenario. The first simulation task is to demonstrate how measurements of multipath fading channels can be done from a system point of view. Another task is a statistical analysis of the capacities of both fixed and mobile WiMAX communication over such channels, whose response varies over both time and frequency in most cases.

The channel measurements are intended to serve as an introduction to practical measurements of multipath channels, and the measurements should only be performed indoor due to resource limitations. The measurement records are to be processed to estimate the RMS delay delay spread of the channel. The objective is not to define general metrics of indoor channels, but rather to demonstrate the process in a practical approach.

1.2 Background

The foundation of this report is the project carried out in the winter semester on the WiMAX standard. This project served as an introduction to WiMAX

and included a thorough theoretical study, accompanied by simplified capacity analysis in Matlab. The WiMAX standard is in fact a set of standards defining the physical and multiple-access protocols of different wireless standards. The standard 802.16-2004 defines the wireless interface of fixed communication, whereas 802.16e is en extension yielding mobile communications. The former standard was comprehensively discussed in the project, while the latter was only briefly reviewed.

The physical layer properties of these two standards concerning the propagation effects of the channel, is the major area of study of this report. The other physical layer features, such as modulation, bandwidths and carrier frequencies, are selected according to the supported parameters of WiMAX. The channel itself is not standardized in the same manner, due to its diverse nature. The selection of the physical layer implementation variables merely depend on the effects of the underlying communication channel, and these parameters are crucial to the achieved capacity and Quality of Service (QoS) offered by the system. Quantifying the effects of wireless multipath channels and a statistical analyzing of the capacities, may serve useful in the prediction of the QoS and overall system capacity.

1.3 Scope

The focus area of this report comprises propagation effects of fixed and mobile multipath channels, principally the effects of multipath signal reception. Only NLOS is considered, i.e. the Rayleigh fading model can be used. A thorough theoretical review is required for fully understanding the concepts and approaches in the Matlab simulations. The simulations serve as a basis for understanding the methods used for channel measurements. Moreover, simulations are present for statistically estimating the capacity of WiMAX over various fixed and mobile multipath channels. The latter part of the report will focus on practical measurements of the multipath channels discussed and simulated in the previous sections. This part is intended to present a guideline and demonstration of how to perform measurements and extraction of metrics of multipath channels.

Standardization of path loss and propagation effects of wireless channels will be broadly discussed, succeeded by a narrow focus on the relevant channel metrics and fading characteristics of multipath channels. The goal is not to lecture the topics, rather to emphasize the features and problems of communicating over such channels. The simulations demonstrate these effects and the limitations of wireless communication over multipath channels.

Measurements are performed with channel sounder equipment developed by Sintef/Telenor R&D. Due to limitations of resources, the measurements are

only performed indoor. Results are analyzed and parameters are extracted in order to calculate the RMS delay spread.

This report is composed of the following chapters: Introduction, Theoretical Aspects, Matlab Simulations, Channel Measurements and Conclusion.

Chapter 2

Theoretical Aspects

2.1 Free Space Path Loss

Path loss is an universal effect of all waves traveling some distance, independent of the nature of the wave. Just as waves across the surface of the ocean or acoustic waves of a whistle tend to diminish, so do electromagnetic waves. The only difference is at which strength the waves are attenuated. The path loss of electromagnetic waves at radio frequencies, directly influence the received power and link budget of the system, which in turn determines the capacity of wireless communication system. Free space path loss refers to the loss of signal strength, omitting the influence by other propagation factors such as absorption, diffraction, obstruction, refraction, scattering, and reflection. The latter factors are not being further explained, as they are implicitly considered in Section 2.4.

The term "free space" originally refers to the vacuum of outer space. Radio waves propagating in air and vacuum experience almost identical path loss, and the term "free space" is therefore also used for air.

Considering a signal transmitted through free space between a transmitter and a receiver separated by distance d at carrier frequency f, the signal travels in a straight line between them. Along its path, it is suppressed by a scale factor related to the distance, i.e. the power density is reduced. This scale factor is square proportional to both distance and frequency. The equation for free space path loss is as follows, where λ is the wavelength and c is the speed of light ($3 \cdot 10^8 m/s$):

$$free\,space\,path\,loss = \left(\frac{4\pi d}{\lambda}\right)^2 = \left(\frac{4\pi df}{c}\right)^2 \tag{2.1}$$

or equivalently

$$free\,space\,path\,loss\,[dB] = 20\log(d) + 20\log(f) - 147.6 \qquad (2.2)$$

2.2 Path Loss Models

2.2.1 Introduction to Path Loss Models

Calculating and predicting the exact channel behaviour are in most cases not practically realizable. Several path loss factors are not readily available to the receiver and transmitter, causing channel response to be undeterminable. The degree of multipath and Doppler, in addition to the attenuation, delay, frequency- and phase offsets of each path, would require exhaustive calculations and a vast amount of information. The path loss must be estimated in other manners. This is where the Path Loss Models plays a part. These are empirical or analytical mathematical formulations, developed for different environments. The analytical models characterize the received SNR as a function of distance, leading to a well defined path loss. This often requires exhaustive calculation using a technique called ray-tracing. This is efficient, but cannot handle complex environments. On the contrary, empirical models of mean received SNR includes the effects of path loss, shadowing and multipath. The former reflects the *large scale path loss* effects caused by the geometry of the propagation, whereas shadowing and multipath depicts *large-scale fading* and *small-scale fading* respectively. The models are a result of signal measurements in different morphological areas and scenarios, and averaged through series of measurement periods and distances. The result is a *local mean attenuation* LMA. The range of such measurements must cover all kind of situations applicable to the specific scenario. Typical variables are frequencies, heights and distances. In a certain type of area, e.g. in a dense city, all variables must be tested within a certain range. A single model is usually developed to predict the behaviour of propagation for all similar links and under similar constraints, causing the model to be heavily dependent upon the radio architecture. Applications of these models are not always restricted to the environments in which the measurements were performed, which in turn may compromise the accuracy when applied to more general environments [1]. Suitable models for parameters other than those used to derive a specific model, can only be established by additional measured data in the new environment. Single-cell architecture with *line-of-sight* (LOS) and no co-channel interference, would need a different set of propagation models than multi-cell systems with LOS or *non-line-of-sight* (NLOS). A number of empirical path-loss models have emerged over the years for predicting the path loss in various environments such as urban macro- and mini-cells, rural areas or indoor. The models to be discussed

have emerged over the years as the most acknowledged outdoor path loss models.

2.2.2 Standards for Empirical Path Loss

Okumura Model

The Okumura Model is one of the most widely used models in large urban macro-cells. Okumura developed a set of curves providing the median attenuation relative to the free space path loss A_{rel}. The curves were developed from extensive measurements of omnidirectional antennas at *base station* (BS) and *mobile station* (MS), and does not provide any analytical explanation. The curves are plotted as functions of distance in the range 1km to 100km from BS, and as functions of frequency in the range 100MHz to 1920MHz. The receiving MS height h_r is 3m and the transmitting BS height h_t is 200m in the curves (Figure 2.1). Correction terms are added to compensate for various heights and terrain types. The model is expressed as

$$L_{med}[dB] = L_{free} + A_{rel}(f, d) - G(h_t) - G(h_r) - G_{area} \tag{2.3}$$

where L_{med} is the median value of the path loss, L_{free} is the free space propagation loss, A_{rel} is the median attenuation relative to free space as found from the curves of Figure 2.1, $G(h_t)$ is the BS height gain factor, $G(h_r)$ is the MS antenna height gain factor, and G_{area} is the gain due to the terrain type found from the curves of Figure 2.2.

The height compensation terms $G(h_t)$ and $G(h_r)$ are given as follows:

$$G(h_t) = 20\log(\frac{h_t}{200}) \qquad 1000m > h_t > 30m \tag{2.4}$$

$$G(h_r) = 10\log(\frac{h_r}{3}) \qquad h_r \leq 30m \tag{2.5}$$

$$G(h_r) = 20\log(\frac{h_r}{3}) \qquad 10m > h_r > 3m \tag{2.6}$$

The Okumura model is considered to be one of the simplest and most accurate in path loss prediction in cluttered environments [2]. Extrapolations of the curves may be done to obtain values outside the measured range, although the validity heavily depends on the circumstances. The model suffers from its slow response to rapid changes in terrain, such as in rural areas, and is therefore only preferred for urban or suburban areas [2].

Hata Model

The Hata Model, also known as the *Okumura-Hata Model*, incorporates the graphical information from Okumura and develops it further to realize the

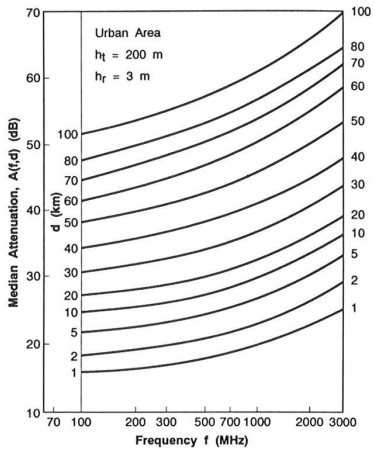

Figure 2.1: Okumura Model: Median attenuation relative to free space over quasi-smooth terrain

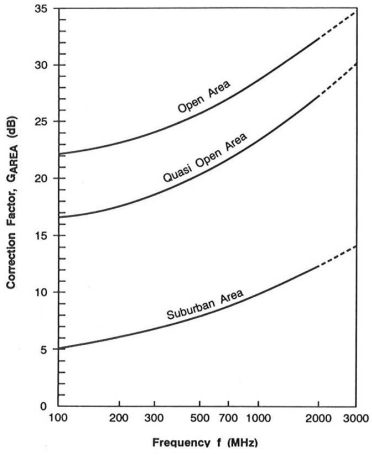

Figure 2.2: Okumura Model: G_{area} correction factors for different terrains

effects of diffraction, reflection and scattering caused by city structures. The model contains two more varieties for open/rural areas and suburban areas, and has an advantage over the Okumura model in its empirical formulation. It covers roughly the same frequency range, i.e. from 150MHz to 1500MHz. The formulation for the median path loss in urban areas is

$$L_{urb}[dB] = 69.55 + 26.16 \log f - 13.82 \log h_t - a(h_r) + (44.9 - 6.55 \log h_t) \log d \tag{2.7}$$

where f is the frequency, h_t is the BS antenna height ranging from 30m to 200m, h_r is the MS height ranging from 1m to 10m, d is the distance from the MS to BS, and $a(h_r)$ is the correction term of the receiver antenna height

as a function of coverage area size. This term is given by

$$a(h_r)[dB] = (1.1 \log f - 0.7)h_r - (1.56 \log f - 0.8) \tag{2.8}$$

for medium sized cities, and for larger cities by

$$a(h_r)[dB] = 8.29(\log 1.54h_r)^2 - 1.1 \qquad for f \leq 300MHz \tag{2.9}$$
$$a(h_r)[dB] = 3.2(\log 11.75h_r)^2 - 4.97 \qquad for f > 300MHz \tag{2.10}$$

The two varieties of the Hata Model yielding median path loss in suburban and open rural areas is respectively given by

$$L_{suburb}[dB] = L_{urb} - 2[\log(\frac{f}{28})]^2 - 5.4 \tag{2.11}$$
$$L_{rural}[dB] = L_{urb} - 4.78(\log f)^2 + 18.33 \log f - K \tag{2.12}$$

where K ranges from 35.94 (countryside) to 40.94 (desert). The Hata model predicts the Okumura model well for $d > 1km$. Hence it is a good model for first-generation cellular systems, but suffers when modeling current cellular systems or indoor environments [1].

COST

COST is a collection of path loss models developed by the *European Cooperation in the Field of Scientific and Technical Research*, referred to as the COST Initiative, due to the limitations in the frequency range of the Hata Model and to the interest in personal communication systems operating at higher frequencies. The first model COST 207, developed in the 80s, contributed to the development of GSM. The follow-up COST 231, developed in the early 90s, assisted the development of HIPERLAN1 and UMTS and the deployment of GSM1800. COST 259 is based on simulations carried out in the late 90s over the disputed access techniques for UMTS, and contributed the deployment of DECT and HIPERLAN2. The recently developed COST 273 deals with more specific issues such as MIMO systems, and the current COST 2100 is an Action on *Pervasive Mobile and Ambient Wireless Communications*. COST encompass more than only path loss issues, and the focus will be restricted to the COST 231 path loss model, commonly referred to as the COST 231 Hata Model.

COST 231 Hata Model is an extension of the Okumura-Hata models, and is designed to be used in the frequency band from 500MHz to 2GHz. The COST 231 model is formulated as

$$L_{urban}[dB] = 46.3 + 33.9 \log f - 13.82 \log h_t - a(h_r) + (44.9 - 6.55 \log h_t) \log d + C \tag{2.13}$$

whereas C is defined as

$$C = \begin{cases} 0dB \text{ for medium cities and suburban areas} \\ 3dB \text{ for metropolitan areas} \end{cases} \tag{2.14}$$

The equations for suburban and open/rural areas are identical to those of Hata (Equation 2.11), and the model is restricted to the following range of parameters: $1km < d < 20km$, $1m < h_r < 10m$, and $30m < h_t < 200m$.

Although the Okumura, Hata and COST 231-Hata models are limited to BS heigths greater than 30m, they are applicable for lower BS heights as well, provided that the surrounding buildings are well below the BS antennas. The COST 231-Hata model it good down to path lengths of 1km, but the path loss becomes heavily dependent upon the local topography for smaller ranges [3].

SUI Models

The SUI Models were developed at Stanford University, and originally defined for the Multipoint Microwave Distribution System (MMDS) frequency band from 2.5GHz to 2.7GHz. The SUI models are defined for three types of terrain, namely A, B and C. Type A is associated with maximum path loss and is applied to hilly terrain with moderate to heavy foliage densities. Type C is associated with minimum path loss and is appropriate to flat terrain with light tree densities, whereas type B is something between. The median path loss is given by

$$L_{med}[dB] = A + 10\gamma \log(\frac{d}{d_0}) + X_f + X_h + s \qquad \text{for } d > d_0 \tag{2.15}$$

where d is the distance from MS to BS, $d_0 = 100m$, and s is a log-normally distributed factor to account for shadowing fading, and has a value between $8.2dB$ and $10.6dB$. The other parameters are defined as

$$A = 20 \log(\frac{4\pi d_0}{\lambda}) \tag{2.16}$$

$$\gamma = a - bh_t + \frac{c}{h_t} \tag{2.17}$$

where h_t should be between 10m and 80m. Note that the parameter γ equals the path loss exponent. The constants a, b and c are given by Figure 2.3. X_f and X_h are correction factors for frequency and height given by

$$X_f = 6 \log(\frac{f}{2000}) \tag{2.18}$$

$$X_h = \begin{cases} -10.8 \log(\frac{h_r}{2000}) \text{ for terrain types A and B} \\ -20 \log(\frac{h_r}{2000}) \text{ for terrain type C} \end{cases} \tag{2.19}$$

Model Parameter	Terrain A	Terrain B	Terrain C
a	4.6	4.0	3.6
b (m^{-1})	0.0075	0.0065	0.005
c (m)	12.6	17.1	20

Figure 2.3: Values of the SUI Model constants a, b and c

2.2.3 Comments on Path Loss Models

Wireless channels cannot be characterized only by mean path loss. The mean path loss only effects the link budget, whereas multipath delay spread/profile, fading characteristics, Doppler spread, as well as adjacent channel- and co-channel interference must be determined to fully characterize the channel. In fixed or nomadic reception, the Doppler spread is quite small. This emphasizes the importance of knowledge of the multipath delay spread/profile and fading characteristics. These terms will be thoroughly discussed in the subsequent sections. More advanced channel models have been developed over the recent years comprising all these effects in multipath mobile environments with MIMO support, such as the extended SUI models. The extended SUI models were embraced by the 802.16 (WiMAX) working group.

It is important to remember that the empirical path loss models are developed by averaging a series of measurement records (stochastic variations are averaged): one clearly cannot expect a single estimation of the path loss to apply to all possible paths between BS and MS. Such predictions can only represent the average value of the path loss, with substantial variations occurring about this mean. The path loss must therefore be treated as a stochastic quantity. Signal fading models can provide statistical description of this behaviour, and will be discussed in Section 2.4. The next section provides the fundamental metrics for understanding the fading concepts.

2.3 Channel Metrics

2.3.1 Delay Profile and Delay Spread

Because of multipath reflections, the channel impulse response looks like a series of dirac delta pulses, referred to as the *Delay Profile*. Under practical conditions, the number of pulses that can be distinguished is very large and depends on the resolution of the measurement or communication system. A single impulse response only reflects a specific scenario of multipath, and this response changes with location as well as time. Fluctuations over location is caused by various relative locations of the scatterers or the receiver/transmitter, whereas fluctuations over time is caused by mobility, i.e. relative speed between transmitter and receiver/scatterers.

The impulse response of a time-variant multipath channel in complex baseband can be expressed as

$$h(t,\tau) = \sum_{i=0}^{N-1} a_i(t) exp(-j\theta_i(t))\delta(\tau, \tau_i(t)) \tag{2.20}$$

where $a_i(t)$, $\theta_i(t)$, and $\tau_i(t)$ is the amplitude, phase shift and excess delay of the ith component at time t. For time-invariant channels, the variable t is simply ignored. This formulation can be interpreted as follows: there are N different paths, i.e. N versions of the same signal arriving at the receiver at time t. Each version experiences different losses resulting in different amplitudes, and different paths result in various phase shifts and excess delays. All three variables are stochastic processes. The phase shift can be assumed uniformly distributed, whereas the amplitude distribution depends on the type of fading (see Section 2.4) in addition to the distance traveled (path loss). The excess delay is normally modeled as Poisson distributed [4]. An example of the impulse response of a time-variant multipath channel is illustrated in Figure 2.4: for a given time t_i, each multipath component has a delay, amplitude and phase.

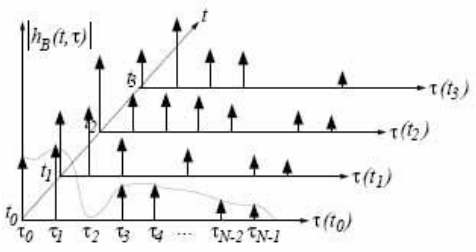

Figure 2.4: Multipath channel impulse response

A commonly used metric for multipath channels is the *Power Delay Profile*. It is illustrated in Figure 2.5 where $P(\tau)$ can be viewed as the channel power spectral density as a function of delay. It is derived from averaging a vast number of channel impulse responses obtained from measurements of a specific scenario.

The *Mean Excess Delay* is the first order moment of the power delay profile:

$$\overline{\tau} = \frac{\sum_i P(\tau_i)\tau_i}{\sum_i P(\tau_i)} \tag{2.21}$$

The Root Mean Square (RMS) *Delay Spread* is defined as the root of the second order moment of the power delay profile:

$$\sigma_\tau = \sqrt{\overline{\tau^2} - (\overline{\tau})^2} \tag{2.22}$$

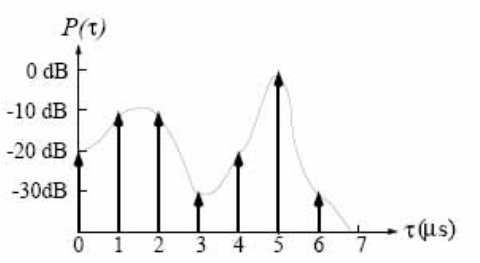

Figure 2.5: Multipath power delay profile

2.3.2 Doppler Spread and Coherence Time

The Doppler Effect is the change in frequency and wavelength of a wave that is perceived by an observer moving relative to the source of waves. Identical to what may have been noticed from the sound of a bypassing train or car, this is also the case for radio signals. For radio waves traveling at the speed of light through air, this change in frequency is given by

$$\Delta f = \frac{fv\cos\theta}{c} = \frac{v}{\lambda} \tag{2.23}$$

where f is the transmitted frequency, c is the speed of light ($3 \cdot 10^8$ m/s), v is the velocity of the receiver (m/s) relative to the transmitter, and λ is the corresponding wavelength. θ is the angle of arrival of the signal relative to the velocity vector as illustrated in Figure 2.6. The Δf of Equation 2.23 is commonly referred to as the *Doppler shift* f_m. The maximum Doppler shift occurs at $\theta = 0°$ and is then only limited by the relative velocity. f_m can be either positive or negative, and the *Doppler Spread* B_D is defined as the two-sided frequency span of f_m, i.e. *Doppler Spread* $= 2f_m$. The channel *Coherence Time* $T_C = 1/B_D$ is the reciprocal of the Doppler Spread, i.e. the time in which the channel impulse response remains constant.

Moreover, the angle of arrival of the reflected components can be viewed as uniformly distributed

$$PDF(\theta) = \frac{1}{2\pi} \tag{2.24}$$

i.e. the Doppler frequency $f_D = f_m \cos\theta$ is cosine distributed. Setting

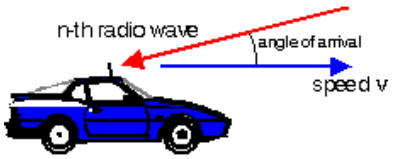

Figure 2.6: Typical Doppler scenario

$f_{rel} = f_D/f_m$ gives

$$\frac{d\theta}{df_{rel}} = \frac{d \arccos f_{rel}}{df_{rel}} = -\frac{1}{\sqrt{1-(\frac{f_D}{f_m})^2}} \tag{2.25}$$

The received power in $d\theta$ around θ is proportional to $\frac{d\theta}{2\pi}$, which results in a *Doppler Power Spectral Density*:

$$S(f_D) \propto \frac{d\theta}{2\pi df_D} = \frac{C}{\sqrt{1-(\frac{f_D}{f_m})^2}} \tag{2.26}$$

This spectrum is illustrated in Figure 2.7.

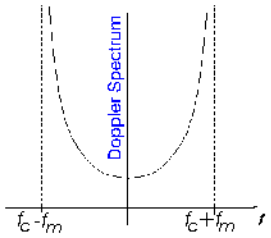

Figure 2.7: Doppler spectrum. f_c = carrier frequency, and f_m =maximum Doppler frequency

2.4 Signal Fading

As mentioned in the previous section, signal fading is the phenomenon of random fluctuations in the received signal level. These may be short-term fluctuations observed over distances of half a wavelength or some time interval, or it may be long term variations in the mean level. Two two phenomenons are caused by multipath effects and shadowing respectively, and are commonly referred to as small-scale fading and large-scale fading. Small scale fading is also caused by movements of the receiver, transmitter or reflectors, i.e. the relative speed between them, causing the time-variance. This effect, called the Doppler effect, is typical in mobile communication systems.

2.4.1 Shadowing

The Shadowing effect may be observed as long term variations in the received signal level. It is caused by movements over distances large enough to cause gross variations in the overall path from BS to MS. A receiver caught in the shadow (relative to the transmitter) behind buildings, hills, and other large

obstacles experiences the shadowing effect. Such effects are also caused by changes in reflecting surfaces and scattering objects.

The received signal mean, i.e. averaged over large distances and time, obtained from an empirical path loss model incorporates both the free space path loss and the average attenuation due to fading. As a consequence, the value found from either of these models is valid as the mean for shadowing considerations. The long term standard deviation of this mean level is due to the shadowing effect. The most common model for this attenuation is log-normal shadowing, which has been empirically confirmed to model the received level accurately in both outdoor and indoor environments [5]. The ratio of the transmitted-to-received power $\psi = P_t/P_r$ is expressed as

$$f(\psi) = \frac{\xi}{\sigma_{\psi dB}\psi\sqrt{2\pi}} exp[-\frac{(10\log\psi - \mu_{\psi dB})^2}{2\sigma^2_{\psi dB}}] \tag{2.27}$$

where $\mu_{\psi dB}$ is the mean of $\psi dB = 10\log\psi$, $\xi = 10/ln10$, and $\sigma_{\psi dB}$ is the standard deviation of ψdB. If an analytical path loss model is used for extracting the mean level, $\mu_{\psi dB}$ must include both the path loss (as obtained from the model) and the average attenuation of the shadowing process. The effect of shadowing is illustrated in Figure 2.8 (b).

2.4.2 Multipath Effects

Multipath is the effect of reflections from buildings, hillsides or even smaller units such as cars and trees, causing several versions of the same signal to arrive at the receiver. These time-delayed and phase shifted rays are added constructively or destructively at the receiver, resulting in fluctuations in received signal amplitude. Movements over small distances such as half a wavelength, may lead to severe variations in signal amplitude. Such fading is therefore called small-scale fading. A broad categorization of small-scale fading due to multipath is *flat fading* and *frequency selective fading*. A signal is said to undergo flat fading when the channel has linear phase response and a constant gain over the bandwidth of the transmitted signal. Under such conditions, the signal might experience variations in channel gain over time due to new locations, but the spectral response over the signal bandwidth remains constant. However, if the channel gain and phase response is not flat over the transmitted signal bandwidth, the signal will suffer from frequency selective fading. In this case the channel response varies over both time (caused by new locations) and frequency. This causes the signal to be dispersed by the channel and results in *Intersymbol Interference* (ISI). The frequency fades are caused by multiple versions of the transmitted signal, attenuated and phase shifted differently, and channel equalization is necessary at the receiver to encounter the frequency fading. If the time delays of the reflected components are small enough (relative to the symbol duration),

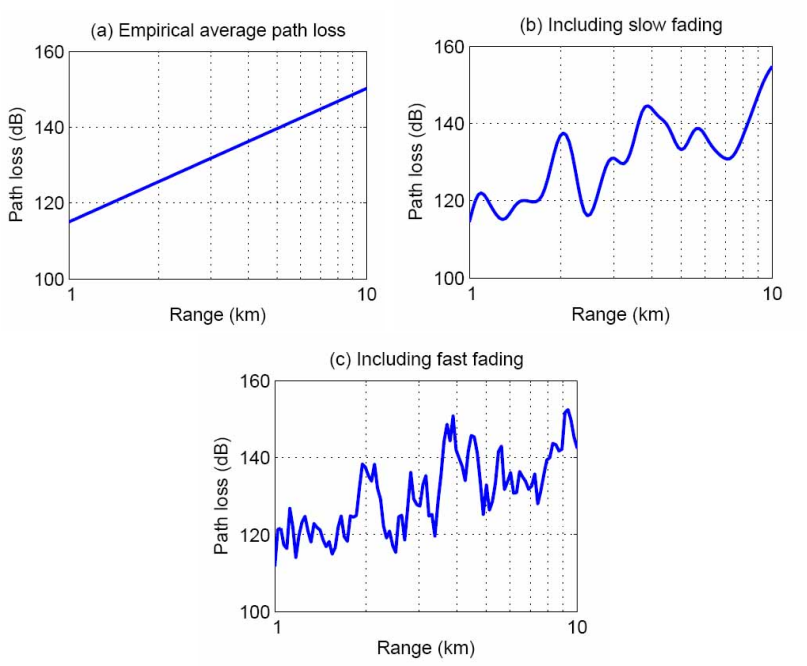

Figure 2.8: Typical path loss behaviours: (a) Average path loss from an empirical model (b) including effects from shadowing (c) superimposed by multipath fading

the channel can be approximated to be flat over the signal bandwidth. A rule of thumb is that the channel may be characterized as flat if $T_{symb} \geq \sigma_\tau$, where T_{symb} is the symbol period and σ_τ is the channel delay spread, and frequency selective otherwise [6]. The effect of multipath fading is illustrated in Figure 2.8 (c).

When a single ground reflection dominates, the two-ray model may be applied. Whereas more complex scenarios need to be solved empirically, this ray-tracing technique provides a good analytical estimate of the received signal amplitude for the two-ray scenario. Figure 2.9 is an illustration of the two-ray scenario, and the channel impulse response can be relatively expressed as

$$h(t) = a_0[\delta(t) + \alpha\delta(t-\tau)e^{j\phi}] \tag{2.28}$$

where a_0 is the attenuation of the LOS component, $\alpha = a_1/a_0$ is the relative attenuation of the ground reflected component, τ is the delay (relative to the symbol period), and ϕ is the phase shift of the reflected component. The baseband frequency response is found by Fourier transform and given by

$$H(f) = a_0[1 + \alpha e^{-j2\pi f\tau}e^{j\phi}] \tag{2.29}$$

which is frequency dependent. In chapter 3, the impulse response of Equation

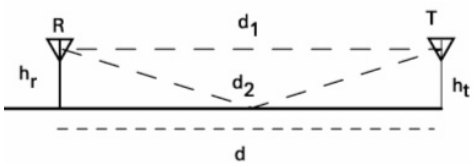

Figure 2.9: Two-ray ground reflection scenario

2.28 is extended to 4 or 6 paths and thoroughly simulated.

2.4.3 Doppler Fading Effects

When there is relative motion between the transmitter and receiver or scatterers, a Doppler Spread B_D is introduced, which effects the received signal spectrum and causes some level of frequency dispersion: the signal of transmitted bandwith $2B$ i broadened to $2B + B_D$. Depending on the relative difference between the transmitted signal bandwidth B_S and B_D, the signal undergoes either *fast fading* og *slow fading*. Fast and slow fading only deals with the rate at which the channel is changing due to motion, and is independent of whether the channel is flat or frequency selective. Fading due to Doppler Spread the other type of small-scale fading, in addition to small-scale fading caused by multipath fading.

Slow Fading

In the case of slow fading, the channel impulse response changes at a rate significantly slower than the transmitted symbol period T_{symb}. The channel is then assumed constant over several consecutive symbol intervals. Equivalently, the Doppler spread of the channel is much less than the bandwidth of the transmitted signal. To summarize, slow fading occurs when

$$T_{symb} \ll T_C \tag{2.30}$$

or

$$B_S \gg B_D \tag{2.31}$$

where B_S is the transmitted symbol bandwidth, and $T_C = 1/B_D$ and B_D is the channel Coherence Time and Doppler Spread respectively.

In flat fading channels, the channel impulse response can be approximated by a single dirac pulse. Slow fading on flat fading channels occurs when the amplitude of the dirac varies at a rate of change much slower than the transmitted symbol period T_{symb}. In case of frequency fading channels, slow fading is experienced when the amplitudes, phases and time delays of any of the multipath components vary slower than T_{symb}.

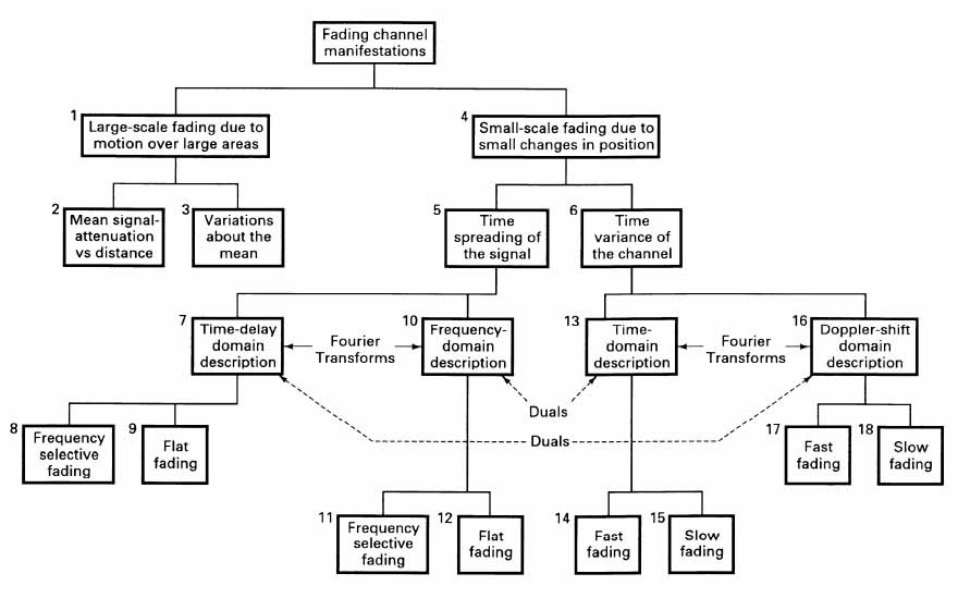

Figure 2.10: The manifestations of fading channels

Fast Fading

Fast fading is said to occur when the Doppler Spread is significant relative to the bandwidth of the transmitted symbol. The frequency dispersion caused by fast fading leads to a signal distortion, which becomes larger with increasing Doppler Spread relative to signal bandwidth. Fast fading is experienced when

$$T_{symb} > T_C \tag{2.32}$$

and

$$B_S < B_D \tag{2.33}$$

As for slow fading, both flat and frequency fading channels can undergo fast fading. A fast fading, flat fading channel is a channel where the amplitude the channel-equivalent dirac impulse varies at a rate of change faster than the transmitted symbol period. A fast fading, frequency fading channel is experienced when the amplitudes, phases and time delays of any one of the multipath components vary more rapidly than the symbol period.

The relationship between large-scale fading (Shadowing) and the four different types of small-scale fading are illustrated in Figure 2.10.

A brief consideration of the link budget for fading channels is illustrated in Figure 2.11. This figure shows the various contributions that must be considered when estimating path loss and margins for mobile channels. The different contributions are:

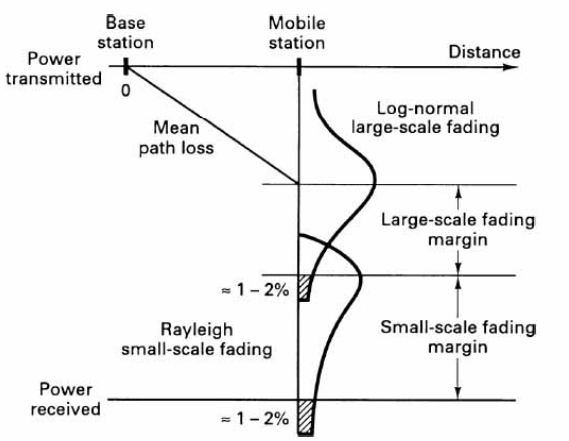

Figure 2.11: Link budget considerations for fading channels

- Mean path loss as function of distance. Normally found from a suitable empirical model
- Large-scale fading (Shadowing). Near worst-case variations about the mean (Typically 6dB to 10dB [7])
- Small-scale fading (Rayleigh, see Section 2.4.4). Near worst-case variations about the mean (Typically 20dB to 30dB [7])
- The annotation "1-2%" indicated a suggested area, or probability, under the tail of each pdf as a designed goal. In other words, the margin provides an adequate received power for approximately 98-99% for each type of fading.

2.4.4 Small-Scale Fading Models

So far, only the classifications and effects of multipath and Doppler have been discussed. Statistical models for small-scale fading for various scenarios exist. For mobile communication over multipath channels, the models for Rayleigh and Rice fading are commonly used.

Rayleigh Fading

In NLOS mobile radio channels, the Rayleigh distribution is often used to describe the statistical time-varying nature of a flat fading channel, or of the envelope of an individual multipath component. In a multipath environment, the received envelope of either path experiences Rayleigh fading. Depending on the relative speed, i.e. the Doppler spread, the rate of change is increased or decreased accordingly. The amplitude, or envelope, of each

reflected component can be represented in terms of its in-phase and quadrature component as $a_{I,i} + ja_{Q,i}$. Because of the wave cancellation effect and random movement, both the in-phase and quadrature components are Gaussian distributed with zero-mean, i.e. $\vec{a} = a_{I,i} + j \cdot a_{Q,i}$ is complex Gaussian distributed [8]. The envelope of the reflected component i is expressed as

$$r_i = \sqrt{a_{I,i}^2 + a_{Q,i}^2} \tag{2.34}$$

The envelope of a complex gaussian distributed variable is Rayleigh distributed [9], which has a pdf given by

$$p(r) = \begin{cases} \frac{r}{\sigma^2} exp(\frac{-r^2}{2\sigma^2}) & \text{for r} \geq 0 \\ 0 & \text{otherwise} \end{cases} \tag{2.35}$$

where σ is the standard deviation. The pdf is plotted in Figure 2.12. The individual paths of a multipath channel suffer from Rayleigh fading in a NLOS environment. When there is a dominant component, i.e. LOS, the Rice model can be used. Simulations for Rayleigh fading multipath channels are found in Section 3.

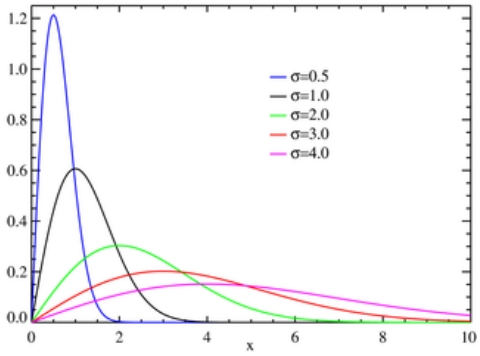

Figure 2.12: Rayleigh PDF

Rician Fading

Whenever there is a dominant stationary signal component (such as LOS, nonfading) present, the small-scale fading envelope distribution can be approximated Ricean. In this case, $a_{I,i}$ and $a_{Q,i}$ of Equation 2.34 for the fixed LOS component are not zero-mean variables. The received signal now equals the superposition of a LOS component and complex gaussian components representing the NLOS contributions. The received signal envelope can be shown to have a Ricean distribution [10] given by

$$p(r) = \frac{2(K+1)r}{\Omega} exp[-K - \frac{(K+1)r^2}{\Omega}] I_0[2\sqrt{\frac{K(K+1)}{\Omega}} r], r \geq 0, K \geq 0, \Omega \geq 0 \tag{2.36}$$

where $I_n(\cdot)$ is the nth order modified Bessel function of the first kind, $\Omega = E[r^2]$ and K (the K-factor) is the ratio of the power received from the LOS component to the power contribution of the NLOS components. For $K = 0$ we have Rayleigh fading, whereas for $K = \infty$ we have no fading. Ricean fading will not be discussed further, as it is beyond the scope of this report.

Chapter 3

Matlab Simulations

3.1 Introduction

This chapter will focus on the implementation and results of the Matlab simulations performed on different aspects of multipath channels. The first section is called "Simulation of Multipath Channel Measurement" and is a system simulation of the multipath channel measurements described in Chapter 4, including the implementation of the multipath fading channel itself. The second section, called "Capacity Simulations" comprises capacity simulations of both fixed and mobile communication over a multipath fading channel.

Simulations were implemented in Matlab 7.0, and require the following toolboxes for operation: "Signal Processing Toolbox" and "Statistics Toolbox".

All simulations use the same base code found in Appendix A.2, whereas the simulation main files are included in Appendix A.1. A thorough system overview is presented in Section 3.2.2 covering the aspects of the implementation from a conceptual point of view. Both simulation main sections contain a subsection called "implementation". The purpose of this subsection is to present a specification of the procedures and functions implemented from a mathematical and conceptual perspective, rather than an in-depth study of the code.

The main purpose for the simulations is to achieve a thorough and more visual understanding of the fading effects of multipath channels explained in Chapter 2, including metrics such as delay profile, delay spread, multipath fading, Doppler spread, and channel capacity. It is important to take notice of the delay profile: this is dynamically generated, i.e. a fixed standardized delay profile is not used.

3.2 Simulation of Multipath Channel Measurement

This program implements the behaviour of the time-varying and frequency selective multipath channel, and simulates how such channels may be measured by transmitting a repetitive *Chirp Signal*. The Section 3.2.2 provides an overview of the implementation from a system point of view, whereas the implementation itself is carefully explained in Section 3.2.3. The simulation results are reviewed in Section 3.2.4, and the main simulation file "measurement_simulation.m" is found in Appendix A.1.1.

3.2.1 The Chirp Signal

A chirp is a signal in which the frequency increases or decreases with time, referred to as "up-chirp" or "down-chirp" respectively. The frequency may increase either linearly, exponentially or in other fashions, but the focus will be on linear chirps since this is used in the measurements described in Chapter 4. It is called a *chirp* signal for the very simple reason: it sounds like a bird when played through a speaker. The linear chirp is suitable for channel measurements since it sweeps equal frequency spans within equal time slots, and has an almost square shaped Fourier transform. The complex *Linear Frequency Modulated* (LFM)chirp is generated by varying the instantaneous frequency $F(t)$ linearly with time $t \in [-T_{chirp}/2, T_{chirp}/2]$: $F(t) = F_{center} + kt$, where T_{chirp} is the chirp duration. The chirp waveform is thus given by

$$s(t) = e^{j2\pi \int_0^t F(t')dt'} = e^{j2\pi(F_{center}+kt)t} \tag{3.1}$$

and

$$k = (F_{stop} - F_{start})/T_{chirp} = W/T_{chirp} \tag{3.2}$$

where $F_{stop} - F_{start}$ is the swept frequency range over time T_{chirp}. Note that the phase varies quadratically while the frequency varies linearly over time.

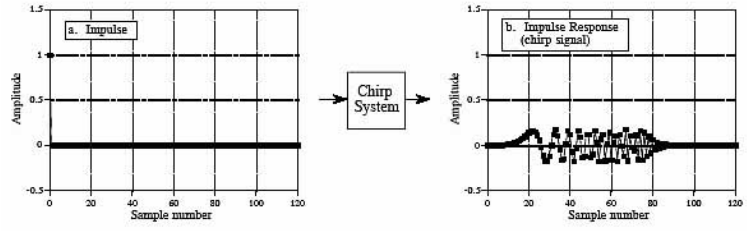

Figure 3.1: Chirp System. The impulse response of the chirp system is a chirp signal

The key feature of the chirp signal is that it is that its completely reversible. If filtered with a filter matched to the chirp itself (*antichirp* filter), the output

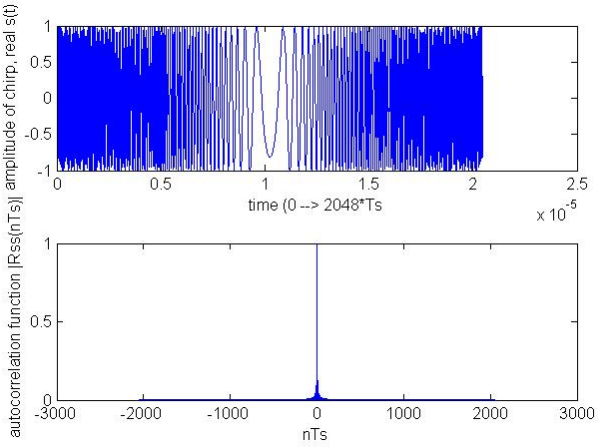

Figure 3.2: Plot of Time Domain Chirp and its Autocorrelation Function

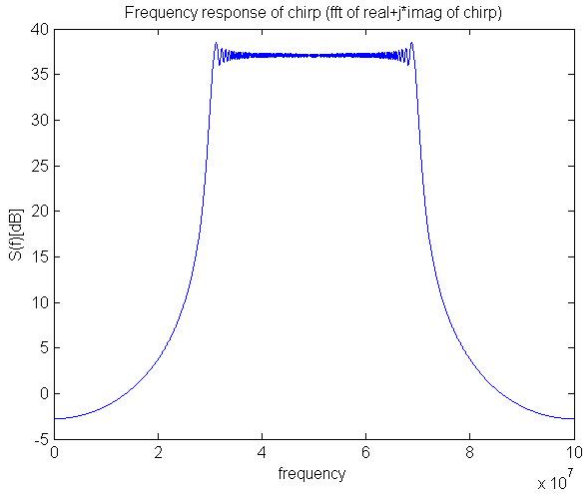

Figure 3.3: Plot of the LFM Chirp Frequency Response

is an impulse. This process equals the autocorrelation estimation of the chirp signal, which generates an impulse at $\tau = 0$. This chain can be viewed as an impulse entering a chirp filter (Figure 3.1), with impulse response given by Equation 3.1, followed by a antichirp filter. The output is an impulse, whose width is given by the sampling frequency of the system when digitalization is necessary (such as in Matlab). A LFM chirp of a given one-sided bandwidth of $W/2$ would, according to the Nyquist criterion, only require a sample frequency of $F_s = 2 * W/2 = W$. But we will need to oversample by at least a factor 5 to properly simulate the continuous signal [11]. The pulse width needs to be as short as possible since it directly reflects the resolution of the system: a $1\mu s$ pulse, i.e. $T_s = 1\mu s$ and $F_s = 1/T_s = 1MHz$, provides a radio burst of about 300m, which means that the distance information

obtained from the system would have the same resolution. Sampling of the continuous chirp with $F_s = 1/T_s$ yields a discrete-time LFM chirp signal (baseband) given by

$$\begin{aligned} s(nT_s) &= e^{j2\pi(F_{center}-kt)t}|_{t=nT_s-T_{chirp}/2} \\ &= e^{j2\pi(0+\frac{W}{T_{chirp}}(nT_s-T_{chirp}/2)^2)} \\ &= e^{\frac{j2\pi W}{T_{chirp}}(nT_s-T_{chirp}/2)^2} \end{aligned} \tag{3.3}$$

for $0 \geq n < T_{chirp}$. The simulation program operates on a LFM chirp of $W = 40MHz$, $F_s = 100MHz$ or $T_s = 10ns$, and a duration of $T_{chirp} = 2048T_s = 2.048\mu s$, i.e. the chirp sweeps from frequency $-20MHz$ to $+20MHz$ in about $2\mu s$ with a distance resolution of $v \cdot t = c \cdot T_s = 3m$. The code for the chirp signal generation and its inverse (the antichirp) is presented in Appendix A.2.2 and A.2.3 respectively. The antichirp is simply the hermitian conjugate transpose of the original chirp signal, i.e. $s^*(-t)$. The whole process of filtering the LFM chirp with its antichirp can be expressed as

$$s(nT_s) * s^*(-nT_s) = \int_{-\infty}^{+\infty} s(\tau)s(\tau + nTs)d\tau = R_{ss}(\tau) \tag{3.4}$$

where $R_{ss}(\tau)$ is the autocorrelation of $s(t)$ in distance τ. In other words, the antichirp filter can be viewed as a *correlator*. This also corresponds to *matched filtering*, i.e. the terms *antichirp filter*, *matched filter* and *correlator* are equivalent.

In the case of a complex LFM chirp transmitted over a flat channel, and convolved with its inverse at the receiver, exactly one impulse is generated as output. This impulse appears as a spike in the time-domain centered around $\tau = 0$ with minor sidelobes. Multiple versions of the LFM chirp of different delays added and filtered in the similar way would output multiple impulses from the correlator at time-locations according to the delays. This is exactly the concept exploited by using chirp signals for multipath measurements, as explained in details in the following sections.

Matlab plots of the time domain LFM chirp, correlator output (chirp auto-correlation) and frequency response of the real and imaginary parts of the LFM chirp are found in Figure 3.2 and 3.3 respectively.

3.2.2 System Overview

A schematic overview of the system simulated is illustrated in Figure 3.4. As explained in the previous section, a chirp signal can be generated by applying a dirac pulse $\delta(n)$ on a filter with impulse response according to Equation 3.3. The sample frequency $F_s = 100MHz$ of the chirp signal spreads the

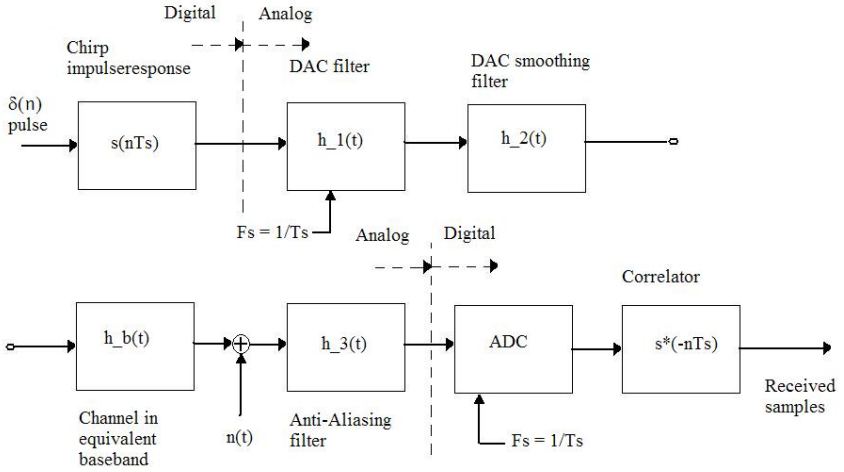

Figure 3.4: Transmitter - Receiver Chain for Channel Measurements

periodic frequency response $S(F)$ of the LFM chirp in frequency, repeating the spectrum every $100MHz$ as in Figure 3.5. The chirp oversampling factor is hence $100MHz/40MHz = 5/2$.

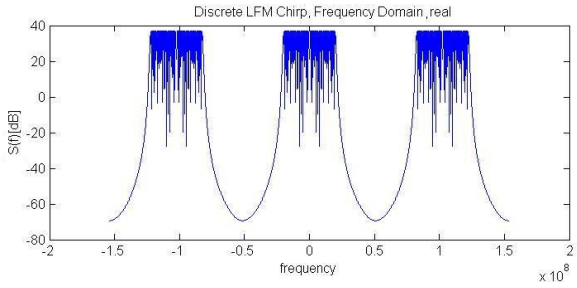

Figure 3.5: Frequency Response of LFM Chirp at $F_s = 100MHz$, real part

The filter h_1(t) is the Digital-to-Analog Converter (DAC), which in the time-domain is a square pulse of duration T_s and unit amplitude given by

$$h\_1(t) = \begin{cases} 1 & \text{for } t \in [0, T_s] \\ 0 & \text{otherwise} \end{cases} \tag{3.5}$$

which is the idealistic DAC impulse response. The smoothing filter h_2(t) follows the DAC. The purpose of h_2(t) is to bandlimit and smooth the output from the DAC. Due to the square shape of the time-domain DAC pulses, the frequency response is a sinc function extending to $+/-\infty Hz$, i.e. it has to be bandlimited. Filter h_2(t) has an effective one-sided bandwidth of $30MHz$, which is enough to limit the bandwidth of the LFM chirp and

to smooth it. At the receiver, an anti-aliasing filter h_3(t) is necessary to remove the aliasing products illustrated in Figure 3.5. The anti-aliasing filter needs an effective one-sided bandwidth of $30MHz$ to remove the aliasing products without distorting the desired LFM chirp.

The cascade of the three filters $g(t) = h\_1(t) * h\_2(t) * h\_3()$ is assumed well approximated by a raised cosine filter with one-sided bandwidth $F_g = 30MHz$. The impulse response of the raised cosine filter is

$$g(t) = [\frac{\sin(\pi t/T_g)}{\pi t/T_g}] \cdot [\frac{\cos(\alpha\pi t/T_g)}{1-(2\alpha t/T_g)^2}] \tag{3.6}$$

where $T_g = 1/(2F_g)$ and $\alpha \in [0,1]$ is the roll-off factor (0.5 is used by default).

The chirp signal is transmitted over the multipath channel expressed by its impulse response h_b(t). This is to be simulated for a suggested number of paths.

A tapped delay line model for the Rayleigh fading multipath channel to be simulated is illustrated in Figure 3.6. Briefly summarized, the N paths experience N different delays and attenuations given by the (generated) delay profile. The Rayleigh fading is uncorrelated between paths, i.e. the paths are statistically independent.

Each path (tap) is composed of an In-Phase (I-channel) and a Quadrature (Q-channel) component, each of which experiences time-correlated fading. It is the envelope of these paths that are modeled as Rayleigh distributed (i.e. Rayleigh fading is experienced). The time-correlated Rayleigh fading is produced by filtering a sequence of complex Gaussian samples through a Doppler filter equal to Figure 2.7 (denoted F(f) in Figure 3.6), i.e. both the I- and Q-channel of a each tap experiences Gaussian distributed fading, but the envelope of the tap itself suffers from Rayleigh fading, as discussed in Chapter 2.4.4. In addition, the output of the Doppler filtering process must have an envelope of unity on average, and thus a scale operation is needed after this process (denoted by the scale factor k_0).

Only the receiver front-end noise at a given time-instance is considered: the thermal noise is assumed minimal in relation to the receiver front-end noise figure.

The simples multipath channel model is the *two-ray model* composed of a direct and a reflected component. In this case, h_b(t) can be expressed as

$$\begin{aligned} h\_b(t) &= a_0 e^{j\phi_0} e^{-j\omega\tau_0}\delta(t-\tau_0) + a_1 e^{j\phi_1} e^{-j\omega\tau_1}\delta(t-\tau_1) \\ &= a_0 e^{j\phi_0 - j\omega\tau_0}[\delta(t-\tau_0) + \frac{a_1}{a_0} e^{j(\phi_1-\phi_0)} e^{-j\omega(\tau_1-\tau_0)}\delta(t-\tau_1)] \end{aligned} \tag{3.7}$$

where τ_i is the delay, a_i is the attenuation and ϕ_i is the phase shift of component i. This can be simplified by setting $\tau_0 = 0$, $a_1/a_0 = \alpha$ ϕ_0,

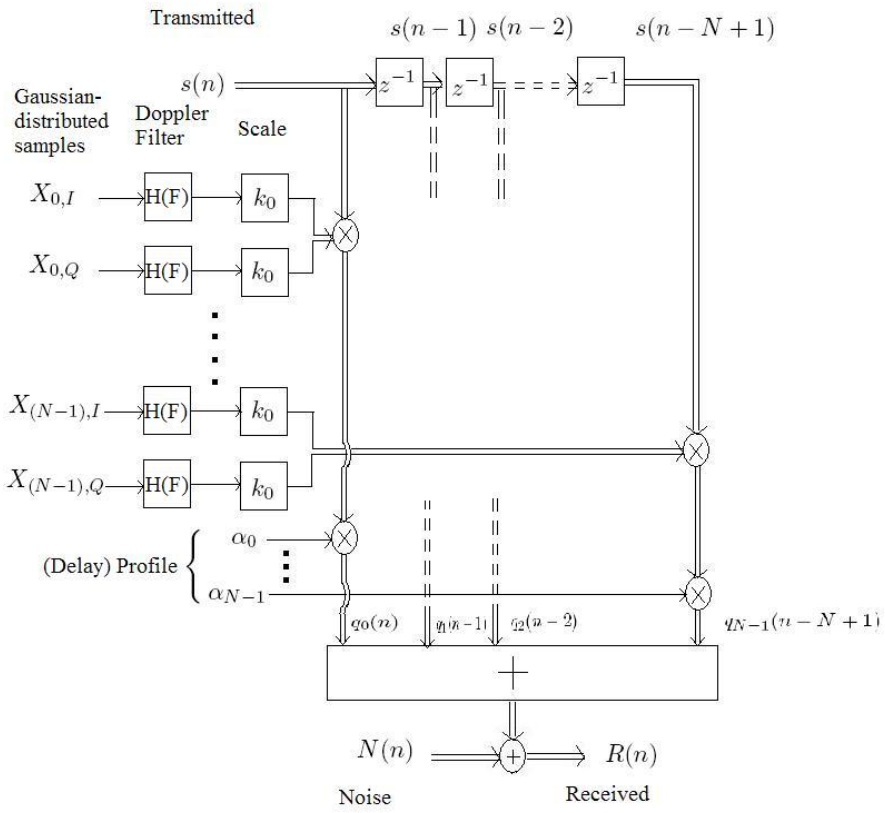

Figure 3.6: System Model of Multipath Rayleigh Fading

indicating that only the relative delay of the components are of interest:

$$h\_b(t) = a_0[\delta(t) + \alpha e^{j\phi_1} e^{-j\omega\tau_1} \delta(t - \tau_1)] \tag{3.8}$$

or in the frequency domain:

$$H\_b(F) = a_0[1 + \alpha e^{j\phi_1} e^{-j\omega\tau_1} e^{-j2\pi\tau_1}] \tag{3.9}$$

h_b(t) can be extended to include any number of paths by adding additional time-delayed terms to Equation 3.7.

The analog chain can thus be modelled as:

$$g_{sys}(t) = h\_b(t) * g(t) \tag{3.10}$$

or

$$G_{sys}(F) = H\_b(F) \cdot G(F) \tag{3.11}$$

Simulating this system in Matlab requires all data to be discretized. The analog chain $g_{sys}(t)$ must thus be sampled at a suitable sample frequency. The LFM chirp generator outputs chirp samples $s(nT_s)$ at a rate F_s. Sampling the analog system function $g_{sys}(t)$ at $F_s = 100MHz$ results in a frequency response of

$$G_{sys,sampled}(F/F_s) = F_s \sum_{k=-\infty}^{+\infty} G_{sys}(F - kF_s) \tag{3.12}$$

Since $G_{sys}(F)$ is bandlimited to $+/-30MHz$, the Nyquist theorem holds and the sampling process introduces no degradation of $G_{sys}(F)$.

The whole system chain can now be modeled in the time domain as

$$x(nT_s) = s(nT_s) * g_{sys,sampled}(nT_s) * s^*(-nT_s) \tag{3.13}$$

Another problem remains: the length of raised cosine function $g(t)$ is infinite, and hence the length of $g_{sys,sampled}(nTs)$ as well. Multiplying $g(t)$ with a windowing function $w(t)$ solves this, but introduces some convolution error in the time domain. If $w(n)$ is sufficiently long, this error can be ignored. Another solution is by performing

$$X(F) = S(F) \cdot G_{sys,sampled}(F) \cdot S^*(F) \tag{3.14}$$

and to take the Discrete Fourier Transform (DFT) of this. The convolution error is minimized by using a large DFT size. The implementation makes use of a square window for time-limitation of $g_{sys,sampled}(nTs)$, i.e. the cos-roll of $g(t)$ is truncated at $+/-8 \cdot T_g$ where T_g is defined in Equation 3.6.

The samples $x(nTs)$ is the correlator output, which can be used to detect the impulse response of the multipath channel as explained in Section 3.2.1.

3.2.3 Implementation

The implementation of the channel measurement simulation is found in "measurement_simulation.m" (Appendix A.1.1) and is the implementation of the system chart illustrated and conceptually explained in the previous section. An important notice to all simulation programs, is that the programs are parametrized, i.e. all parameters of importance are initialized in a global parameter file called "global_variables_initialize.m" (Appendix A.2.1). The initialization is performed in the beginning of all simulation programs. Two important parameters are defined in the simulation program itself: *NPath* and *comtype* defining the number of taps (reflected paths) and whether the communication is mobile or fixed. *References will be made to the system charts illustrated in Figure 3.4 and 3.6.*

Channel and System Filter

The cascade of the multipath channel h_b(t) and the system filter g(t) (Equation 3.6), excluding rayleigh fading and noise, is generated in the function "channel_filter_cascade.m" (Appendix A.2.4). As mentioned in the previous section, this system filter is an approximation of the cascade of the three filters h_1(t), h_2(t) and h_3(t) by a raised cosine filter. The multipath channel h_b(t) can be specified by any given number of paths, and each path experiences independent phase shift, attenuation and delay:

- The phase shifts experienced within each path is assumed to have a rectangular probability distribution from 0 to 2π.
- The delay is given relative to the first arriving component. The first component therefore experiences zero relative delay, whereas the consecutive components arrive at time-instances of a fraction of the total chirp symbol duration $T_{chirp} = 2048 \cdot T_s$, normalized by T_{chirp}. This fraction (before normalization) is set to be within the window $1 \cdot T_s$ to $128 \cdot T_s$, and is selected randomly. The reason for these limits is that a the delay must be small compared to the symbol duration fro successful ISI mitigation, such as the *cyclic prefix* used in WiMAX OFDM. On the other hand, the delay is not set to be smaller than $1 \cdot T_s$ due to the resolution limitation given by sampling frequency $F_s = 1/T_s$. A relative delay of $\tau = 1 \cdot T_s$ equals a path distance difference of 3m, whereas $\tau = 128 \cdot T_s$ equals 384m, which will be sufficient for the measurement scenario to be performed in Chapter 4. The delay can be any fractional multiple of T_s (within the given interval) in implementation of the channel. However, for the system model illustrated in Figure 3.4, this delay must equal an integer multiple of T_s.
- The attenuation, i.e. the mean attenuation in absence of fading, of each path is related to the delay encountered. The attenuation of the first arriving component, i.e. the path with $\tau = 0$, is normalized to 1, whereas all other paths are attenuated logarithmically corresponding to the delay:

  $$a_i = 1/\log(10 + n_i) \tag{3.15}$$

  where a_i is the attenuation of path i and n_i is the corresponding delay expressed between 1 and 128. The formula above was generated as an example for suitable visualization of the measurement simulation.

Succeeding the creation of the multipath channel impulse response h_b(t), the convolution with the raised cosine system filter g(t) impulse response is performed. The code for creating a raised cosine filter is given in Appendix A.2.5, which implements Equation 3.6. This convolution, given two paths, can be expressed as

$$h\_b(t) * g(t) = g(t) + a_1 e^{j\phi_1 - j\omega_c \tau_1} g(t - \tau_1) \tag{3.16}$$

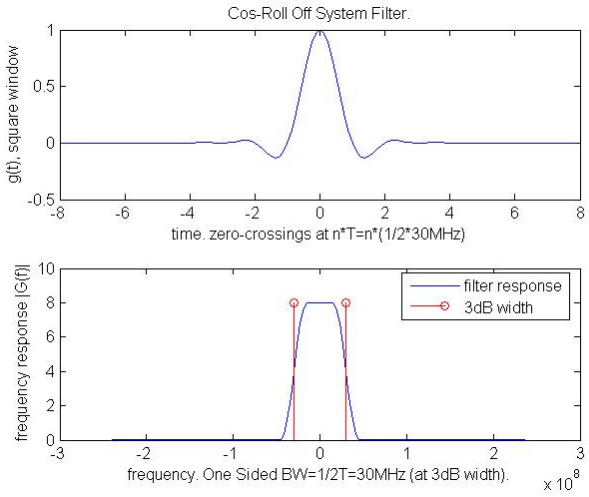

Figure 3.7: Raised Cosine System Filter. One-sided BW is 30MHz and roll-off factor α is 0.5

which is implemented in equivalent baseband. The raised cosine filter is plotted in Figure 3.7. Note that the time-domain version is truncated at +/-8T. At this point, the amplitude level has dropped below 1% (0.42%) of the maximum level, and the error introduced by square-windowing at this point is minimal and is therefore ignored.

A example of the cascade of g(t) (Figure 3.7) and the multipath channel impulse response h_b(t) is plotted in Figure 3.8. This was generated using 4 paths, and in absence of Rayleigh fading. Note that the 4 components are delayed and scaled versions of g(t), sampled at time instances T_s. The multipath channel itself is illustrated in Figure 3.9

Fading

Each path in the multipath channel model encounters independent fading according to Figure 3.6. An important distinction needs to be made, namely whether the communication is *mobile* or *fixed*. For mobile communication, the receiver moves with some velocity relative to the transmitter, resulting in Doppler shifts. The broadening of the received spectrum due to these shifts were stated in Section 2.3.2. For fixed communications, Doppler shifts are also experienced due to movement of the scatterers. The overall distribution of such Doppler shifts can be approximated Gaussian [12], [13]. The difference between the two, is simply the Doppler filter $H(F)$ applied, illustrated in Figure 3.6:

- In mobile communications, this filter has a frequency response given

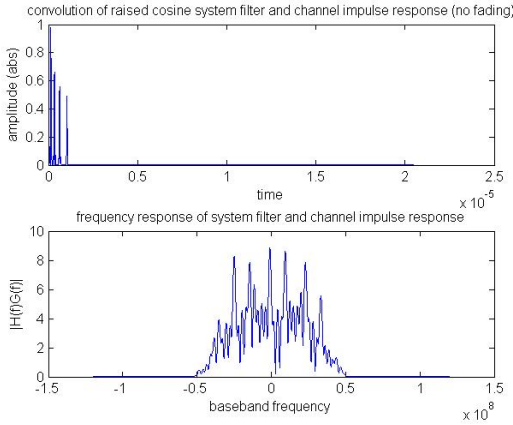

Figure 3.8: Cascade of System Filter and Channel given 4 Paths

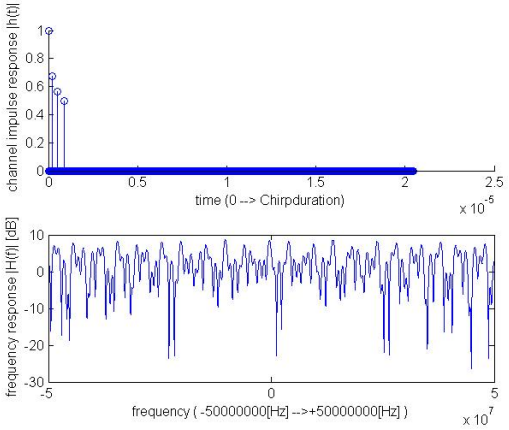

Figure 3.9: Multipath Channel given 4 Paths

by Equation 2.26. The implementation is found in Appendix A.2.6, where the maximum Doppler frequency is set to $F_m = 50Hz$. At carrier frequency $f_c = 2.1GHz$, $v = f_m \cdot \lambda \approx 7m/s$, i.e. 50Hz is a suitable for normal walking. The process of Doppler filtering, resulting in the fading coefficients for the first path, is illustrated in Figure 3.10.

- In fixed communication, the Gaussian distributed Doppler filter is selected with a cut-off at $3 \cdot \sigma = F_m = 50Hz$, i.e. the probability of Doppler shifts exceeding $3 \cdot \sigma$ is minimal. The Gaussian Doppler filtering and the output of the filtering process is illustrated in Figure 3.11, whereas the code is appended in A.2.7.

Common for both scenarios, is that a sequence of complex Gaussian samples are applied to the filter (Doppler or Gaussian Doppler filter). The filtering process correlates the samples according to the filter bandwidth. A wide filter bandwidth, i.e. a large maximum Doppler shift, results in less correlation

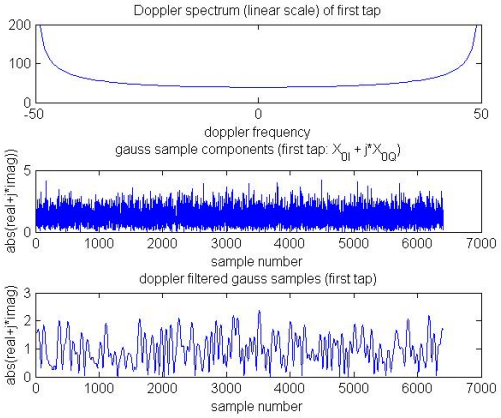

Figure 3.10: Doppler Filtering Process and Fading Coefficients. Mobile Communication.

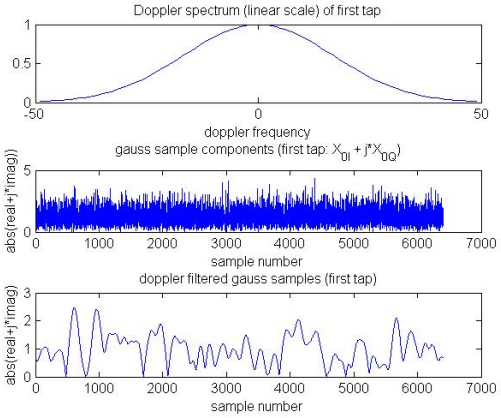

Figure 3.11: Gaussian Doppler Filtering Process and Fading Coefficients. Fixed Communication.

(fast variations), whereas a narrow bandwidth results in the opposite. This can be seen from the rate of variation between succeeding samples of the filtered output.

The correlation of the Doppler filtered samples reflects the time-correlation of the fading within each path. For the mobile case, the filtered samples in the lower plot of Figure 3.10 must be defined by some sample duration $T_{s,doppler}$. The duration of these samples reflects the speed of the fading process. The chirps transmitted in this simulation has a duration $T_{chirp} = 2048 \cdot T_s = 20\mu s$. The Doppler filter two sided bandwidth 100Hz corresponds to a Coherence Time of 0.01s. For suitable visualization of the fading effects, *the chirps are transmitted with a time-separation of 0.01s*, and the duration $T_{s,doppler}$ is set to 0.01s as well. In other words, each transmitted chirp experience a new

fade level (a new Doppler filtered sample is applied to the chirp). The same principle applies to the fixed scenario.

Chirp and Noise Generation

The chirp signal and the antichirp used in the receiver correlator is generated according to the equations and illustrations of Section 3.2.1.

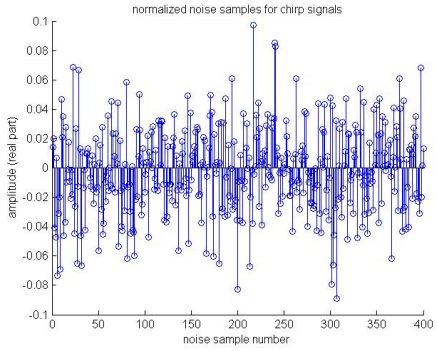

Figure 3.12: Real Part of Generated Noise Samples ($\sigma_{noise} = 0.1$ and zero mean)

Noise is added independently to each received component due to independent noise at different time-instances of arrival. Since the only noise considered is at the receiver front-end, the thermal noise added in each path of the channel is ignored as mentioned in the previous section. The noise computed is a realization of stationary complex Gaussian noise, with a mean and standard deviation as follows: The realization of the stationary noise produces noise samples, these samples must be scaled to represent suitable noise sample amplitudes. The mean value of the samples is still 0, but the standard deviation σ_{noise} must be scaled to correspond to a suitable SNR limit. The SNR limit is set to 20dB (according to QAM-64 transmission as explained in Section 3.3.1). The only purpose of the noise in these simulations, is the illustrate the variations of the system output, and hence the exact noise amplitude is of minor relevance. Assuming an average received signal amplitude of unity, this results in $\sigma_{noise} = 0.1$.

The noise samples are generated in the function "generate_noise.m" (Appendix A.2.8) and scaled by σ_{noise}. This random noise is plotted in Figure 3.12, where 4 paths and 100 transmitted chirps have been simulated.

Simulating the Chain for Consecutive Chirps Transmitted

The measurement simulation itself is now performed by transmitting a certain number of chirps, with intervals of 0.01s (equals the Channel Coherence Time as explained previously in this section), across the time-varying multipath channel. It is time-varying due to the multiplication of each path with independent fading coefficient *sequences* generated by the Doppler filtering process. The rate at which these coefficients change determines the speed of the fading process, and each path of each transmitted chirp is multiplied with one fading coefficient (whereas the next chirp is multiplied with the subsequent fading coefficient). This means, that the channel cannot be assumed constant from one transmitted chirp to the next, but can be assumed constant within the chirp duration. For slower fading, the fading coefficients could be interpolated, or decimated for increased speed. For illustration purposes, interpolation is not performed to fully illustrate the time-variety over a relatively small number of succeeding chirp signals. This means that the channel is slow fading according to Equation 2.30. The number of consecutive chirps to be transmitted is set by the global variable Measurement_duration (= 100 chirps by default), i.e. 100 chirps are transmitted in intervals. This number is small, but sufficient to illustrate the time-varying fading of the system output. In the measurements performed in Section 4, a vast number of chirps are transmitted continuously, and averaging 16 consecutive chirps is performed as an attempt to mitigate the noise. However, averaging is omitted in these simulations, and the number of chirps is limited by the simulation performance and visibility of the effects on the simulation plots.

The simulation loops the transmission of 100 Chirp signals and stores the output of the correlator. A short pseudocode of this implementation is presented:

```
components = find(all components of channel_filter_cascade)
for each chirp
  for each component
    if fixed communication
      fadingcoeff = next gauss doppler-filtered sample according to Fast_Fading_Ts_factor
    elseif mobile communication
      fadingcoeff = next doppler-filtered sample according to Fast_Fading_Ts_factor
    end
    component = component*fadingcoeff + next_noise_sample
  end
  apply components to channel_filter_cascade
  output(chirp_index)=ifft(fft(chirp)*fft(channel_filter_cascade).*fft(antichirp))
restore channel_filter_cascade
end
calculate average RMS delay spread.
```

Each delayed component of each chirp experiences fading according to *fadingcoeff* and noise is added. The fading coefficient and noise sample is only updated if the component processed is part of a new distinct path, i.e. sidelobe-samples due to the system filter cascade experiences the same fading and noise for a given appurtenant path.

The system output is generated in the frequency domain (FFT), and inversely Fourier transformed (IFFT). The delay spread of the channel can be calculated from the output, and a plot of the time-domain behaviour of the channel is performed.

3.2.4 Simulation Results

Mobile Communication

The simulation of the scenario for a fixed transmitter and mobile receiver was performed with the following parameters: $F_s = 1/T_s = 100MHz$, Chirp_duration $= T_{chirp} = 2048 \cdot T_s$,
Chirp_onesided_BW $= 20MHz$, Approximated_system_filter_onesided_BW $= 30MHz$, Approximated_system_filter_rolloff $= \alpha = 0.5$ and Measurement_duration $= 100 \cdot T_{chirp}$. The number of paths (NPath) is set to 6. The output of the correlator (i.e. the system output) is plotted in Figure 3.13, 3.14 and 3.15, where it is possible to observe the independent fading and delay of each path, and the introduced noise (realization of the stochastic noise process) at the time-instance of each received component.

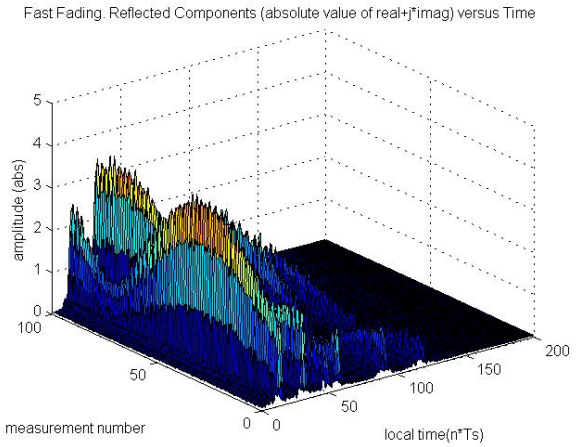

Figure 3.13: System Output: Measured Channel Profile versus Time (Mobile Simulation)

The transmitted chirp is identical to Figure 3.2 and 3.3, whereas the system filter has already defined and illustrated in Figure 3.7.

The generated "unknown" multipath channel before fading is introduced is plotted in Figure 3.16, and the cascade of this channel and the system filter is illustrated in Figure 3.17. The latter is the the ideal average output of the correlator. The delay, phase shift and amplitude of each path of the generated channel is displayed in the Matlab console:

```
DELAY RELATIVE TO duration:
   relative delay of the first arriving component is 0
   relative delay of reflected component 2 is 0.0086259
   relative delay of reflected component 3 is 0.016385
   relative delay of reflected component 4 is 0.020348
   relative delay of reflected component 5 is 0.037219
   relative delay of reflected component 6 is 0.050678

RELATIVE PHASE DIFFERENCE OF FIRST AND SUBSEQUENT REFLECTED COMPONENTS:
   phase of the first arriving component is 0
   phase of reflected component 2 is 4.1962
   phase of reflected component 3 is 0.085617
   phase of reflected component 4 is 3.5285
   phase of reflected component 5 is 2.8561
   phase of reflected component 6 is 5.686

RELATIVE ATTENUATION:
   relative attenuation, a0, of the first arriving component is 1
   attenuation of reflected component 2 is 0.69351
   attenuation of reflected component 3 is 0.61011
   attenuation of reflected component 4 is 0.58368
   attenuation of reflected component 5 is 0.51663
   attenuation of reflected component 6 is 0.48636
```

where the delay is given as $n \cdot T_s/(2048 \cdot T_s) = n/2048$ (n is any value between 1 and 128), and the rest is explained in the "Channel and System Filter" part of Section 3.2.3.

As may be observed from the system output (Figure 3.13), the amplitude level of each path varies over time. This is due to the Rayleigh fading generated by the Doppler filtered gauss samples multiplied with each signal component. The shape of the fading of the output is identical to the correlation between consecutive samples from the Doppler filtered samples, as seen from Figure 3.18 and 3.19 compared to the first tap of Figure 3.13

The measured channel impulse response is now time-varying, and the RMS Delay spread is calculated for each output of the correlator according to Equation 2.22. These RMS Delay spread values are used to produce the time-averaged RMS Delay spread, which is printed in the Matlab console:

```
RMS Delay spread for 6 paths is: 42.4836*Ts (Ts = 10ns)
```

which corresponds to 127 meter.

This simulation has illustrated the possibility of multipath fading channel measurements, as being performed in Chapter 4, and the effects of mobile reception.

Fixed Communication

An identical simulation has been performed for fixed communication, i.e. the receiver and transmitter are at fixed locations. The only difference is the fading caused by the movement of the scatterers, resulting in frequency dispersion according to the Gaussian Doppler spectrum of Figure 3.11. Only the simulation output, multipath channel profile and fading coefficients will be considered, whereas the other components have already been considered.

The system output is plotted in Figure 3.20, 3.21 and 3.22. This is quite similar to the output for the mobile scenario. Since most of the Doppler frequency shifts are centered around zero, the fading is slower than the fading experienced in the mobile simulation, i.e. the Gaussian Doppler filtered samples are more correlated as seen from Figure 3.25 and 3.26. It is also worth mentioning that the fading is still Rayleigh distributed (as explained in Section 3.2.2), since complex Gaussian samples are input to the Gaussian Doppler filtering process, as for the mobile scenario. The superimposed noise is also visible in the system output. .

The multipath channel generated in this simulation comprises components of the following parameters, as displayed in the Matlab console:

```
DELAY RELATIVE TO duration:
   relative delay of the first arriving component is 0
   relative delay of reflected component 2 is 0.0045529
   relative delay of reflected component 3 is 0.018123
   relative delay of reflected component 4 is 0.030275
   relative delay of reflected component 5 is 0.058135
   relative delay of reflected component 6 is 0.06197

RELATIVE PHASE DIFFERENCE OF FIRST AND SUBSEQUENT REFLECTED COMPONENTS:
   phase of the first arriving component is 0
   phase of reflected component 2 is 3.5261
   phase of reflected component 3 is 4.0987
   phase of reflected component 4 is 4.8549
   phase of reflected component 5 is 0.66712
   phase of reflected component 6 is 0.0067442
```

```
RELATIVE ATTENUATION:
   relative attenuation, a0, of the first arriving component is 1
   attenuation of reflected component 2 is 0.77754
   attenuation of reflected component 3 is 0.59767
   attenuation of reflected component 4 is 0.5384
   attenuation of reflected component 5 is 0.47376
   attenuation of reflected component 6 is 0.46807
```

The cascade of the channel and the system filter, and the channel impulse response itself it plotted in Figure 3.24 and 3.23. The system output successfully detects all multipath components, accompanied by the noise and fading of each path.

As for the mobile simulation, the RMS Delay spread is calculated and displayed in the Matlab console:

```
RMS Delay spread for 6 paths is: 47.7952*Ts (Ts = 10ns)
```

which corresponds to 143 meter.

The multipath fading channel and the measurement process of multipath fading channels have now been successfully simulated for both mobile and fixed reception. Next up is the capacity simulation of WiMAX 256-OFDM on such channels for both fixed and mobile communication.

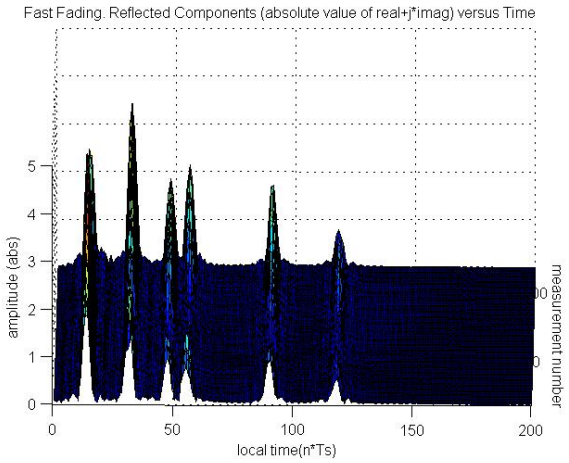

Figure 3.14: System Output: Measured Channel Profile versus Time, Rotated version of Figure 3.13 (Mobile Simulation)

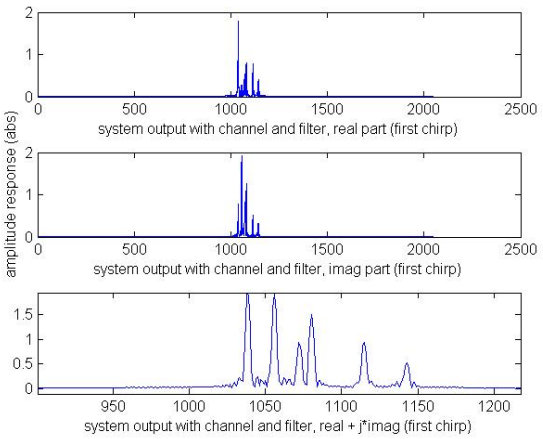

Figure 3.15: System Output: Measured Channel Profile of the first chirp. The bottom plot is zoomed for illustration purposes (Mobile Simulation)

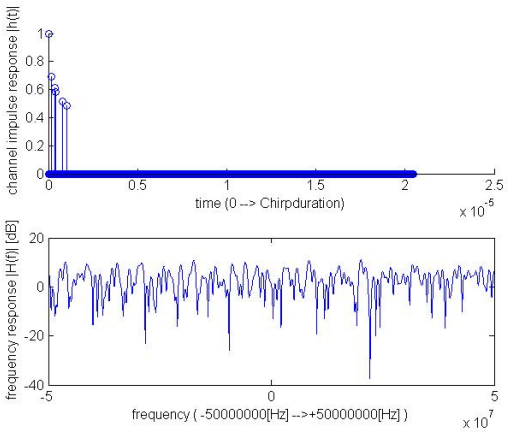

Figure 3.16: Generated Multipath Channel, 6 paths before fading (Mobile Simulation)

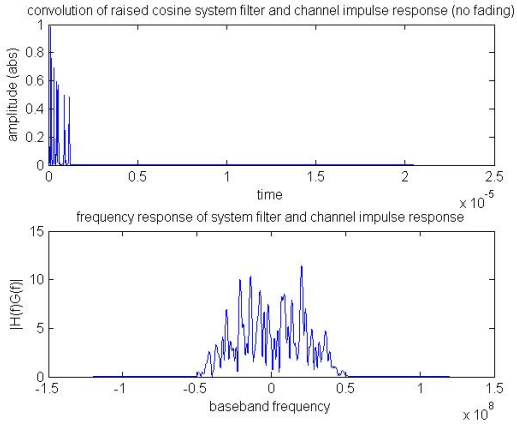

Figure 3.17: Cascade of the Multipath Channel and System Filter, 6 paths before fading (Mobile Simulation)

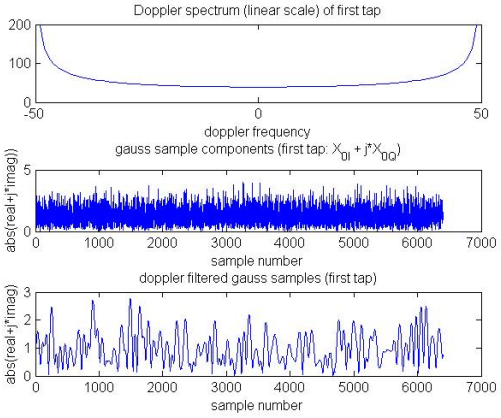

Figure 3.18: Doppler Filter, Gauss Samples and Doppler Filtered Samples for the First Tap (Mobile Simulation)

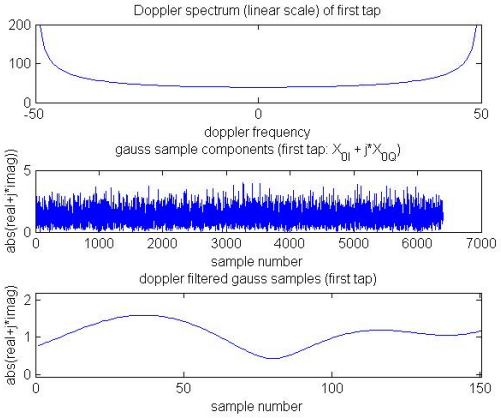

Figure 3.19: Same as Figure 3.18, but the lower plot is zoomed in on the 150 first samples for comparison with Figure 3.13 (Mobile Simulation)

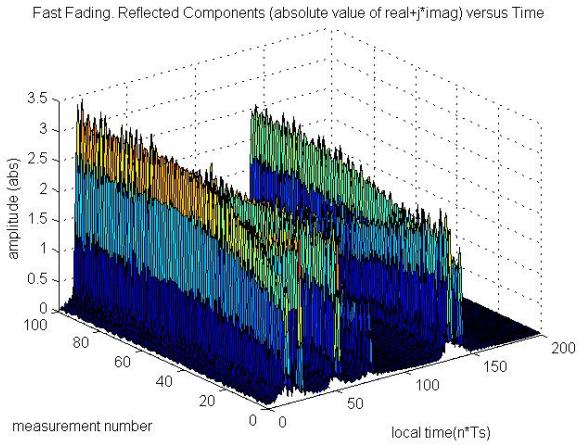

Figure 3.20: System Output: Measured Channel Profile versus Time (Fixed Simulation)

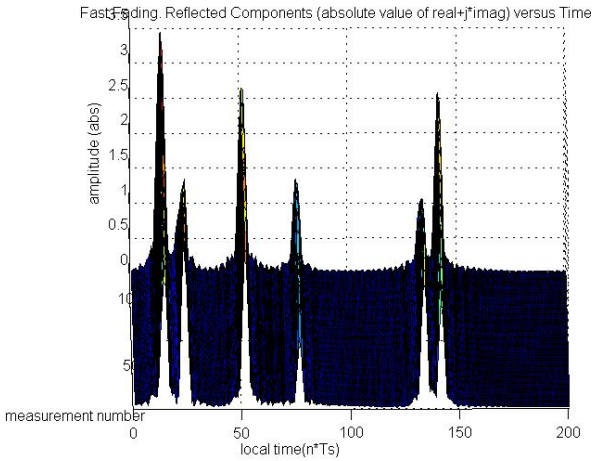

Figure 3.21: System Output: Measured Channel Profile versus Time, Rotated version of Figure 3.20 (Fixed Simulation)

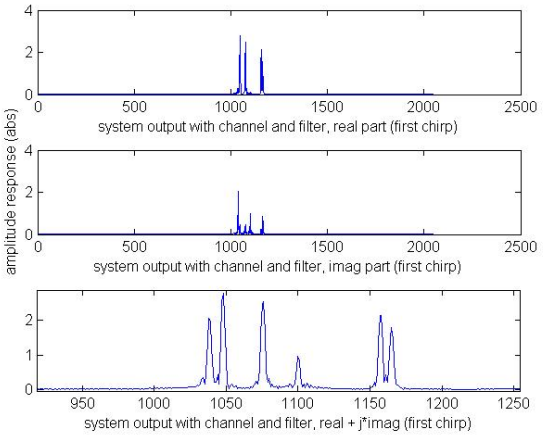

Figure 3.22: System Output: Measured Channel Profile of the first chirp. The bottom plot is zoomed for illustration purposes (Fixed Simulation)

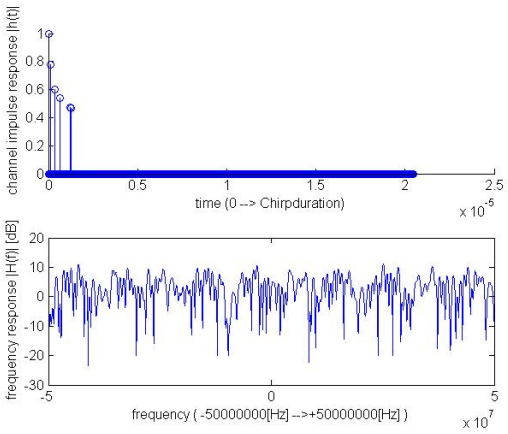

Figure 3.23: Generated Multipath Channel, 6 paths before fading (Fixed Simulation)

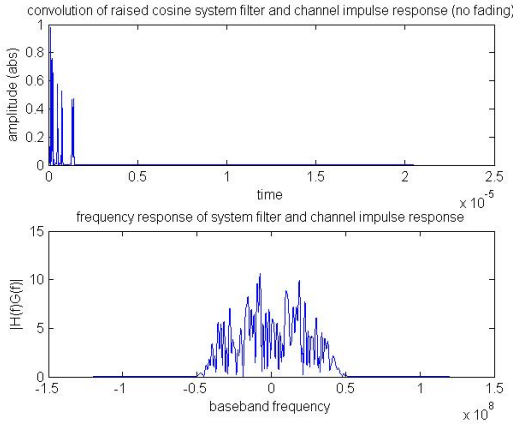

Figure 3.24: Cascade of the Multipath Channel and System Filter, 6 paths before fading (Fixed Simulation)

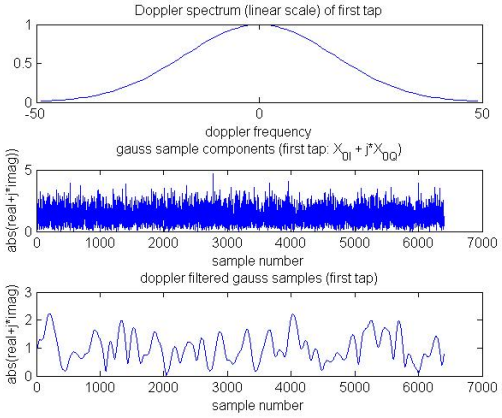

Figure 3.25: Gaussian Doppler filter, Gauss samples and filtered samples for the first tap (Fixed Simulation)

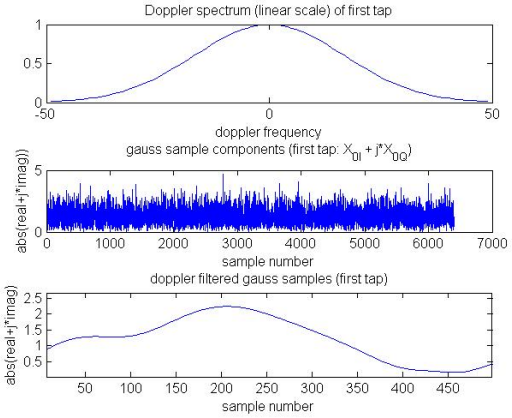

Figure 3.26: Same as Figure 3.25, but the lower plot is zoomed in on the 500 first samples for comparison with Figure 3.20 (Fixed Simulation)

3.3 Capacity Simulations

3.3.1 Introduction and Parameter Settings

The goal of the capacity simulations is to estimate the CDF of the capacity of WiMAX 256-OFDM. WiMAX is a set of standards (802.16) used in the 4G networks currently being established in many countries. It uses OFDM multicarrier modulation with a scalable number of subcarriers. The modulation method to be simulated is 256-OFDM, i.e. 256 subcarriers. The simulation program "capacity_simulation.m" is found in Appendix A.1.2, and uses the parameters set in global_variables_initialize.m (Appendix A.2.1). Four other adjustable parameters of importance are defined in the beginning of the simulation program: NPath, channel_type, NMeasurement and NOFDM. NPath is the number of paths in the multipath channel to be generated, channel_type defines whether the communication is mobile or fixed, NMeasurement is the number of capacity measurements (default: 1000), and NOFDM is the number of subcarriers. The latter is 256 by default, but can be adjusted to 512 or 1024.

One more parameter is defined as well: ignoreFading. This can be adjusted for simulating a non-fading AWGN channel (flat). It is set to include fading by default.

The OFDM symbol transmitted contains no data. It is simply used to define the frequency allocations of the data-subcarriers, pilot-subcarriers and null-subcarriers (guards). The data-subcarriers are defined by a transmitted amplitude of unity, whereas pilot- and null-subcarriers are defined by an amplitude of 2 and 0 respectively. The frequency spacing between subcarriers is 10.94kHz ([14]). The capacity is calculated from the received SNR at the different frequencies of the subcarriers, based on Table 3.1. WiMAX uses adaptive modulation and coding, and the SNR levels for transitions between these were found in [14]. The received SNR is analyzed according to a suggested link budget (adjustable) defined in Table 3.2. This link budget has been adapted from [15], and adjusted to fit the scenario. In addition, the SNR estimation at the receiver is assumed perfect, and equal average transmitted power is assumed in all frequency sub-bands.

3.3.2 Implementation

The implementation starts off by defining the parameters previously described. Each estimation of the channel capacity assumes that the channel has changed, i.e. the spatial distance or time between each measurement is sufficient to allow for assumption of independent channels. The term "channel" is in fact the cascade of the system filter and the multipath channel as in Equation 3.10.

Modulation	Coderate	SNR Level
BPSK	1/2	3dB
QPSK	1/2	6dB
QPSK	3/4	9dB
QAM16	1/2	12dB
QAM16	3/4	15dB
QAM64	1/2	18dB
QAM64	2/3	20dB
QAM64	3/4	21dB
QAM64	5/6	23dB

Table 3.1: List of modulation and coderate used at various received SNR levels, found in the 802.16-2004 standard [14]

Link Budget Parameters	Value	Comment
TRANSMITTER		
Transmit Power Per Element	10dBW	
Transmit Antenna Combination Gain	3dB	Two antennas
Transmit Antenna Gain	8dB	
Pilot Power Boosting Gain	-0.7dB	5/6 of subcarriers used for data
EIRP	20.3dBW	Sum of the TX parameters
RECEIVER:		
Receiver Antenna Gain	0dB	Mobile Antenna
Receiver Antenna Combination Gain	0dB	Only one antenna used
Receiver Noise Figure	6dB	Front-end noise
RECEIVER GAIN	-6dB	Sum of the RX parameters
NOISE:		
Noise Thermal Density	-194dBW/Hz	
System Bandwidth	64.5dBHz	256 carriers,10.94kHz freq spacing
TERMAL NOISE	-129.5dBW	Sum of noise parameters
MARGINS:		
Interference Margin	2dB	
Shadowing Margin	6dB	
Penetration Loss	0dB	Outdoor
SUM MARGINS	8dB	Sum of the margins
PATH LOSS	130dB	About 30km at 2.4GHz
SNR BEFORE CHANNEL FADING	5.8dB	

Table 3.2: Link Budget. SNR BEFORE CHANNEL FADING is 5.8dB, i.e. the channel fade margin is 2.8dB given lower SNR limit of 3dB (BPSK, Table 3.1). The resulting SNR (SNR BEFORE CHANNEL FADING) of this link budget have been numerically found to fit a probability of outage of less than 1%, which is calclulated in the capacity simulations.

A sequence of fading coefficients is generated by calling "doppler_filter.m" (Appendix A.2.6) or "gaussian_doppler_filter.m" (Appendix A.2.7) for mobile and fixed communication respectively. The simulation program has to be run individually for mobile and fixed communication capacity estimations.

The Simulation Loop

A new channel is generated for each measurement. This is done by calling "channel_filter_cascade.m" (Appendix A.2.4) subsequently. The channel consists of a number of paths (defined by NPath) including the time-domain sidelobes generated by the system filter cascade. The components (taps) of the channel impulse response are located, each of which experiences independent fading. Note that the sidelobes of each delayed signal experience the same fading and noise as the belonging signal itself. A sequence of fading coefficients has already been generated, whose contents depend on whether fixed or mobile communication simulation has been selected. A random sample from the this sequence is drawn, constituting the fading coefficient of path k at measurement instance n ($n \in [1, NMeasurements]$). The channel is now updated with a new fade level for each path.

The noise level has already been incorporated in the link budget, assuming equal noise for each capacity measurement and sub-band.

The frequency response of the channel is now analyzed at each OFDM data-subcarrier frequency location to calculate the capacity in bits, omitting the frequency locations of the pilot-subcarriers and null-subcarriers. The received power level is calculated as:

$$\begin{aligned} ReceivedSNR(freqindexk) = \; & ChannelFrequencyResponse(freqindexk) \\ + \; & SNR\_NO\_FADING \end{aligned} \tag{3.17}$$

where SNR_NO_FADING is determined by the link budget (Table 3.2). The Channel Frequency Response superimposes SNR_NO_FADING, resulting in the Received SNR (in presence of small-scale fading). Note that large-scale fading (Shadowing) has been incorporated in the link budget, i.e. the term "fading" in the simulations only refers to the small-scale fading generated by multipath and Doppler shifts.

$ReceivedSNR(freqindexk)$ is compared against the SNR boundaries of Table 3.1 and the Capacity of the current measurement is updated with the number of bits transmitted with the given modulation and coderate pair at frequency index k. For example, QAM16 1/2 rate is capable of transmitting $4 \cdot 0.5 = 2 databits/symbol$. The total capacity over the OFDM bandwidth for each measurement is stored in bit/s as:

$$Capacities(n) = Capacity/OFDM\_Symbol\_Duration \tag{3.18}$$

where n denotes the measurement number, and $OFDM\_Symbol\_Duration = 102.9 \cdot 10^{-6}s$.

The program outputs plots (such as the capacity CDF), in addition to calculating the mean, standard deviation and range of the measured capacities.

3.3.3 Results and Analysis

Flat AWGN Channel

The capacity metrics of a flat AWGN channel need to be found for comparison with the multipath fading channel. The capacity of the flat channel in absence of fading was simulated with the default parameters already mentioned. For the channel to be flat, NPath in set to 1. In other words, the channel has a constant gain and linear phase over a bandwidth greater than the signal bandwidth. Fading is omitted (ignoreFading=1) in order to simulate a time-invariant channel. The term "flat" refers to the multipath channel itself. Anyhow, the frequency response of the cascade between the multipath channel and system filter will not be flat. This is illustrated in Figure 3.27.

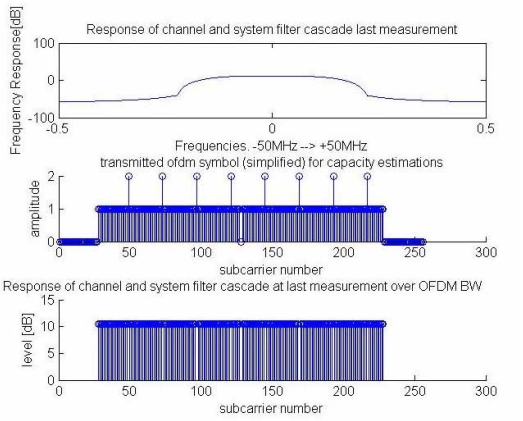

Figure 3.27: Flat AWGN channel: system response, transmitted OFDM symbol, system response over OFDM bandwidth

Figure 3.28 shows the maximum and minimum received SNR levels over the OFDM bandwidth. Note that these are equal, which is natural in a flat non-fading environment. The flat channel is thus time-invariant, resulting in a time-invariant capacity. One measurement would thus be sufficient to estimate the capacity (NMeasurement=1). The capacity metrics are displayed in the Matlab console:

```
CAPACITY METRICS:
```

```
Mean value:5597667.6385bit/s
Standard deviation:0bit/s
Maximum measured capacity:5597667.6385bit/s
Minimum measured capacity:5597667.6385bit/s
Maximum theoretical capacity(QAM64 5/6 rate over all carriers):9329446.0641bit/s

Number of data carriers:192
Number of data carriers below 3dB averaged over 10 measurements is:0
This gives an outage probability of 0%
```

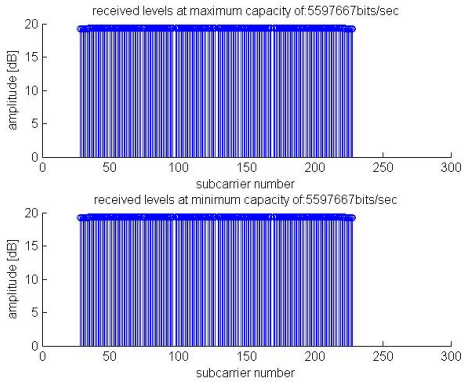

Figure 3.28: Flat AWGN channel: Maximum and Minimum received SNR levels over OFDM bandwidth

Multipath Fading Channel: Fixed Communication

The capacity simulation for fixed communication over multipath channels was performed with the default parameters given in Section 3.3.1 and with 4 independent paths (NPath=4). The system response is now highly frequency dependent, as seen from Figure 3.29. Anyway, the variations are only moderate across the OFDM symbol bandwidth.

The capacity metrics output, based on 1000 measurements, are given as:

```
CAPACITY METRICS:
Mean value:7347769.6793bit/s
Standard deviation:1491727.9615bit/s
Maximum measured capacity:9329446.0641bit/s
Minimum measured capacity:1982507.2886bit/s
Maximum theoretical capacity(QAM64 5/6 rate over all carriers):9329446.0641bit/s

Number of data carriers:192
Number of data carriers below 3dB averaged over 1000 measurements is:1.53
```

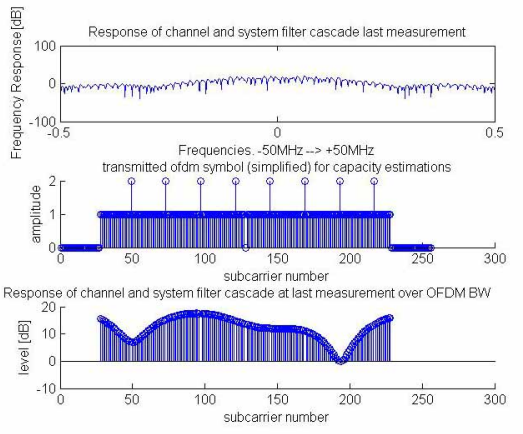

Figure 3.29: Fixed Communication Capacity Simulation: system response for 4 paths, OFDM symbol and response over OFDM symbol bandwidth

```
This gives an outage probability of 0.79688%
```

The capacity mean value has increased in comparison to the flat channel. Multiple signal components are now combined, thus increasing the average received SNR (more energy is obtained). This might suggest that the simulated channel (frequency selective, time-variant) is favorable over the flat time-invariant channel (only LOS) of Figure 3.27. This will only be the case if the fading is slow enough for the feedback channel to provide exact channel estimates, and if the receiver equalization is of sufficiently good quality. The received levels at the minimum and maximum measured capacities are plotted in Figure 3.30.

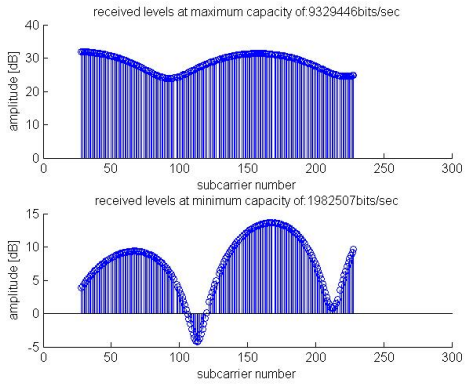

Figure 3.30: Received signal levels over the OFDM bandwidth at maximum and minimum capacity (Fixed)

The capacity is a statistical parameter as a consequence of the statistical

channel, leading to fluctuations across the mean value. Numerical approximations to the capacity CDF and PDF are plotted in Figure 3.31 and 3.32 respectively. The capacity mean solely depends on the link budget. As mentioned, this link budget has been based on a preferred outage probability around 1%. Reducing the received SNR of the link budget (SNR BEFORE CHANNEL FADING), displaces the peak of the capacity PDF to the left, i.e. reduces the mean value and increasing the outage probability. A plot of the capacity PDF after lowering the Transmitter Gain from 12dB to 6.5dB is plotted in Figure 3.33, where the shape reflects the amplitude distribution of the fading coefficients (gaussian doppler filtered, whose envelope is Rayleigh distributed) in dB and quantized according to Table 3.1. The mean capacity is then reduced to 4.6 Mbit/s, and the outage probability exceeds 3%.

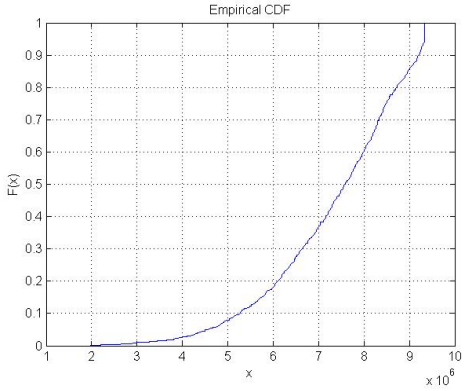

Figure 3.31: Capacity CDF (Fixed)

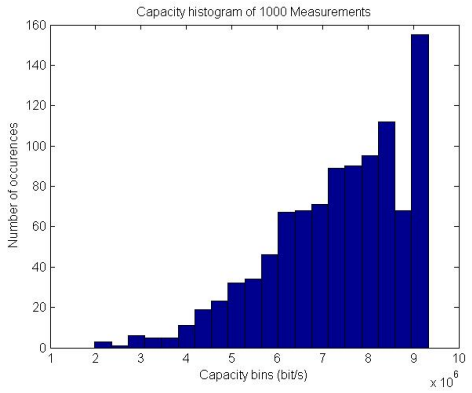

Figure 3.32: Capacity PDF (Fixed)

The peak of the capacity PDF (Figure 3.32) is a result of the upper modulation and coderate limit at 23dB (QAM64 5/6 coderate). All received levels above this threshold, contribute to the total capacity by an equal amount.

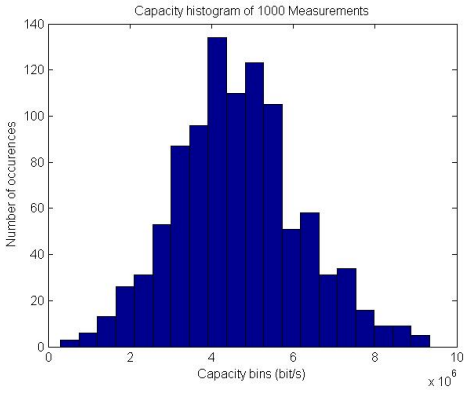

Figure 3.33: Capacity PDF after reducing Transmitter Gain from 12dB to 6.5dB (Fixed)

Multipath Fading Channel: Mobile Communication

A simulation for the mobile scenario was performed with the exact same parameters as in the fixed scenario recently described. The capacity metrics output were:

```
CAPACITY METRICS:
Mean value:7296015.5491bit/s
Standard deviation:1507201.6472bit/s
Maximum measured capacity:9329446.0641bit/s
Minimum measured capacity:2371234.208bit/s
Maximum theoretical capacity(QAM64 5/6 rate over all carriers):9329446.0641bit/s

Number of data carriers:192
Number of data carriers below 3dB averaged over 1000 measurements is:1.858
This gives an outage probability of 0.96771%
```

The capacity of mobile communication is almost identical to the corresponding fixed communication scenario, except for a minor increase in the outage probability. The latter is a result of the previously stated effect of more rapid fluctuation of the fades in mobile communication, as may be observed when comparing Figure 3.18 and 3.25.

The capacity CDF and PDF are illustrated in Figure 3.34 and 3.35 respectively. A plot of the capacity PDF after lowering the link budget Transmitter Gain from 12dB to 6.5dB is plotted in Figure 3.36, where the shape reflects the amplitude distribution of the fading coefficients (Doppler filtered, whose envelope is Rayleigh distributed) in dB and quantized according to Table 3.1). The mean capacity is then reduced to 4.8 Mbit/s, and the outage

probability exceeds 4%. As for the fixed communication simulation, the peak of the capacity PDF is a result of the threshold for QAM64 with 5/6 coderate (at 23dB).

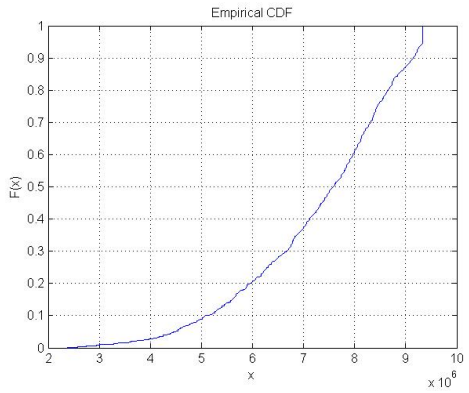

Figure 3.34: Capacity CDF (Mobile)

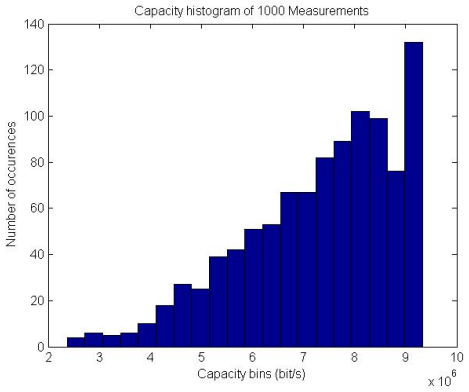

Figure 3.35: Capacity PDF (Mobile)

The received SNR limits at the instances of achieved maximum and minimum capacity is plotted in Figure 3.37, whereas the system response is illustrated in Figure 3.38

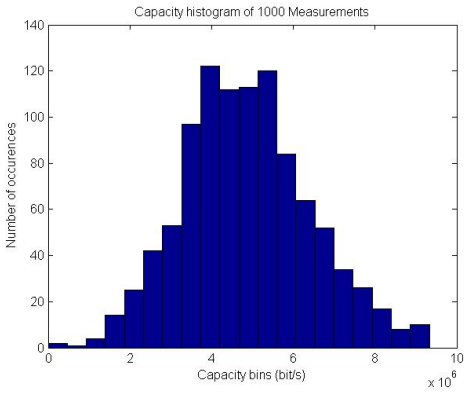

Figure 3.36: Capacity PDF after reducing Transmitter Gain from 12dB to 6dB (Mobile)

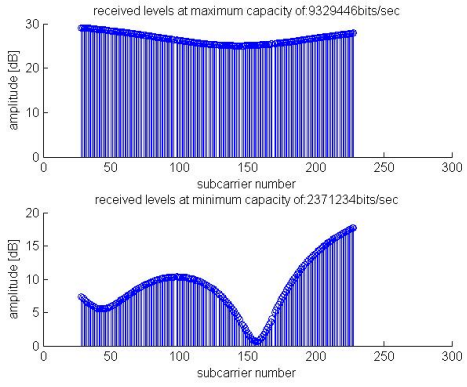

Figure 3.37: Received signal levels over the OFDM bandwidth at maximum and minimum capacity (Mobile)

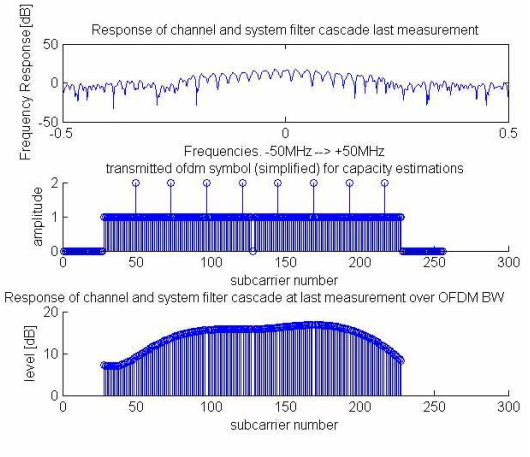

Figure 3.38: Mobile Communication Capacity Simulation: system response for 4 paths, OFDM symbol and response over OFDM symbol bandwidth

Chapter 4

Channel Measurements

4.1 Objective and Scope

The objective of the multipath channel measurements is to introduce the equipment and techniques used in practical multipath channel measurement, allowing these channels to be statistically classified and modeled. The measurement equipment is the channel sounder hardware and software developed by Sintef and Telenor R&D (former Telenor FoU), specified in Section 4.2.

Multipath channels are of statistical nature, and the channel metrics for a given scenario must be found numerically. Measurements of the channel within a range of parameters at a sufficient amount of measurement points, may be used to extract link design parameters suitable for all other similar scenarios. The measurements performed are not intended to be suitable for any relevant channel modeling, rather to emphasize the possibilities and procedures of the process, and to acknowledge the operation of the equipment.

The measurements of the multipath channel were originally aimed at the range of application of the 802.16 WiMAX standards. WiMAX operates in the ISM frequency bands at 2.4GHz and 5.8GHz as well as other licenced bands, and aims both indoor and outdoor operation. The measurements should cover some aspects of the WiMAX physical channel. Due to resource limitations, only indoor measurements came into consideration. The indoor measurements were performed in the corridors of the university, more specifically in the 4th floor of the C-block at Elektrobygget, NTNU, spring 2007. The results were used to estimate the RMS delay spread for this specific scenario. Simulation of the measurement process have been performed in Section 3.2, and the system overview of Figure 3.4 and 3.6 illustrates the measurement system chain and the channel subject to measurements.

The range of measurement frequencies are limited to a chirp bandwidth of

100MHz at carrier frequency of 5.255GHz. This is close to a possible operational frequency range of WiMAX, and measurement results could be interpolated to assert the exact range of WiMAX. Anyhow, the scope of the measurements performed in this scenario is not sufficient, either in range of locations or number of measurements, to encompass any practical utility value for WiMAX. As already mentioned, the results are only used for illustrative and procedural purposes.

4.2 Equipment

4.2.1 Brief Overview

The channel sounder consist of a transmitter sending a known LFM chirp signal, and a receiver which analyzes the received waveform, and stores the processed information to measurement files. The main purpose is to analyze time-variant multipath channels, but other channels may as well be investigated.

The RF modules are designed to cover a 100MHz bandwidth around either 2.1GHz or 5.255GHz, while the IF modules are build to cover a signal bandwidth of 500MHz. The equipment is also capable of performing delay-Doppler measurements, direction of arrival or MIMO measurements by synchronously controlling the antenna switches at transmitter and receiver.

The receiver and transmitter are synchronized by GPS disciplined rubidium oscillators, allowing for simultaneous receiver and transmitter antenna switching within one microsecond, and Doppler shift measurements down to fractions of one Hertz. GPS can also be used to log transmitter and receiver position.

The channel sounder is highly modular and flexible, and can easily be configured for different measurement scenarios. All parameters are controlled in a parameter setup file.

4.2.2 Hardware

The transmitter hardware profile is illustrated in Figure 4.1. It consists of a compact PCI (cPCI) rack with control processor, GPIB controlled Arbitrary Waveform Generator (AWG) and open slots for inserting RF converters etc. The AWG controller software is programmed to generate linear chirps only, although the AWG could output any waveform.

The hardware profile of the receiver is illustrated in Figure 4.2. The receiver is built upon another cPCI rack with control processor, 2 channel acquisition card and a 2 channel IF unit of 10MHz to 500MHz bandwidth and 60dB

range controllable attenuation. As with the transmitter rack, extra slots for inserting RF units are present.

Both the receiver and transmitter rack have a programmable trigger card, synchronized by the GPS assisted rubidium frequency reference source. This is necessary for synchronized antenna switching (MIMO measurements) and data acquisition over several seconds, while maintaining frequency and phase coherence between the receiver and transmitter. An external RF oscillator is needed for RF frequency generation.

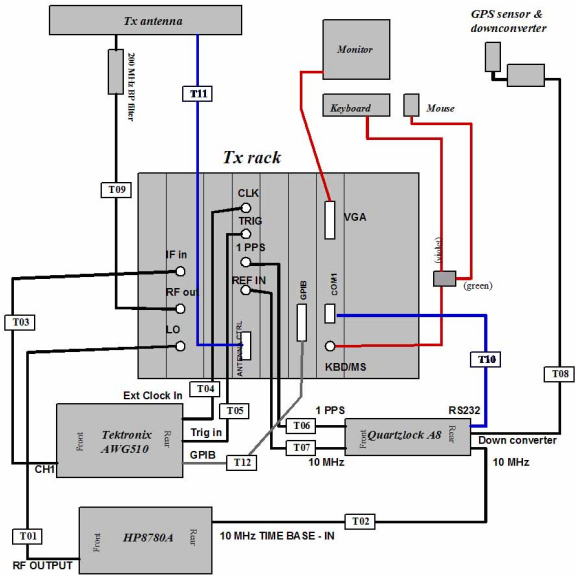

Figure 4.1: Channel Sounder Transmitter Hardware

Transmitter

- **Compact PCI rack**: This is of type GS784-08250C2 from "TreNew Electronic GmbH" and is equipped with
  - PC card (CT7P847 from SBS Technologies) with: 850MHz Pentium II, 256 Mbyte RAM, Ethernet, 4Mbyte graphic controller, IDE and SCSI interface, serial and parallel ports, USB, mouse, keyboard and monitor input.
  - SCSI disk (18.2GB)
  - SCSI CD ROM
  - Floppy
  - GPIB interface card
- **Trigger Card**: Tailor made, and used to trigger signals to the AWG and to generate antenna control signals. It has a realtime clock, syn-

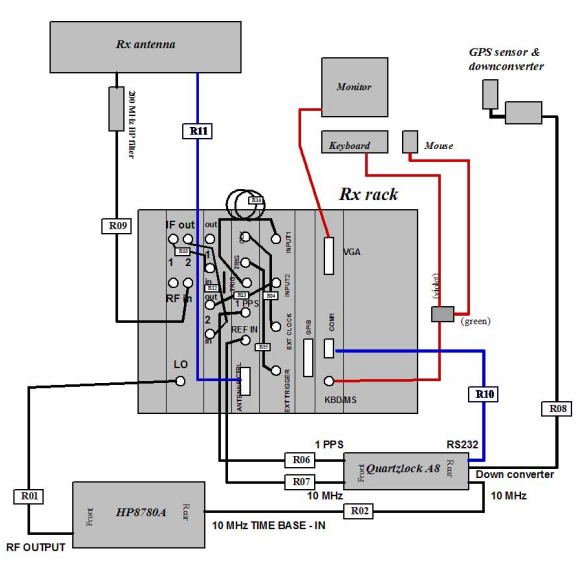

Figure 4.2: Channel Sounder Receiver Hardware

chronized by a 1 pulse per second signal from the GPS assisted rubidium clock. All trigger card frequencies are controlled by a 10MHz frequency reference, also provided by the GPS assisted rubidium source.

- **RF card**: Two RF cards are provided with the equipment: 2.1GHz and 5.255GHz. The latter is used in the measurements and specified as:
  - Input signal center frequency of 125MHz (IF centre frequency)
  - Output center frequency of 5.255GHz (to Tx antenna)
  - Signal BW of 100MHz
  - 50Ω input and output impedance
  - Maximum output level of -33dBm
  - Input IF level between -10dBm and +5dBm
  - Needed local oscillator signal: 5130MHz, 10dBm
- **AWG**: Of type AWG510 from Tektronix. 1GHz sample rate, and fully controllable via Ethernet or GPIB connection.
- **GPS assisted reference clock with antenna**: Of type Quartzclock A8R-Rb. It has a rubidium oscillator as reference, tuned by signals received from GPS satellites through the antenna (antenna be mounted with LOS to the satellites). This reference oscillator needs to be stabilized for some time (up to 24 hours for maximum stability). The antennas might be disconnected after stabilization, and the oscillator will remain in synchronism while the power remains switched on. The

oscillator delivers the 10MHz reference frequency to the trigger card, as well as the 1 pulse per second signal used by the trigger card to synchronize the real-time clock.

- **RF local oscillator**: Not included in the equipment. The oscillator used is of type HP 8672A, set to output 5130MHz at 10dBm signal level to the RF card.
- **Keyboard, mouse and monitor**: Connected to the cPCI rack, and used to control and monitor the system.

Receiver

- **Compact PCI rack**: Same as transmitter, but with a SCSI CD writer
- **RF card**: Two RF cards are provided with the equipment: 2.1GHz and 5.255GHz. The latter is used in the measurements and specified as:
  - Input signal center frequency at 5.255GHz (from Rx antenna)
  - Signal BW of 100MHz
  - 50Ω input and output impedance
  - Maximum input level of -20dBm
  - Amplification: 27dB
  - Noise Factor: 2.5dB
  - Output signal center frequency of 125MHz (IF frequency)
  - Needed local oscillator signal: 5130MHz, 13dBm
- **IF card**: Has a BW of 10MHz to 500MHz. Controllable amplification in 4dB steps over a 60dB range (-14dB to +46dB). The Noise Factor is 6.5dB, and maximum output level is +8dBm.
- **Sampler card**: Of type DC240 from Acuiris. It has two input channels, external clock and trigger inputs. Maximum input bandwidth is 500MHz, and maximum sampling rate is 2GHz. But when used together with trigger card (i.e. external clock), the maximum sampling frequency is 500MHz.
- **RF local oscillator**: Not included in the equipment. The oscillator used is of type Wiltron 69237A, set to output 5130MHz at 13dBm signal level to the RF card.
- **GPS assisted reference clock with antenna**: Same as transmitter.
- **Keyboard, mouse and monitor**: Same as transmitter.

4.2.3 Software

A software overview of the channel sounder is provided in Figure 4.3. A controlling PC might be used to control either Transmitter or Receiver software.

This feature is not utilized, and will thus not be explained. The software modules will only be superficially described.

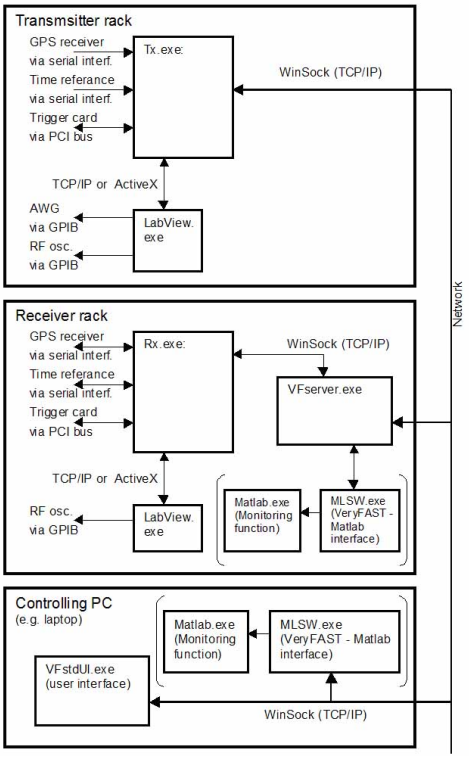

Figure 4.3: Channel Sounder Software Overview

- **Transmitter**: *Tx.exe* is the interface to the transmitter hardware components. Its purpose is setting up the system, interacting with modules during measurements (controlling data flow), and performing the necessary signal processing. This program is started when measurements are to be performed, given a start-time specified in the user interface (VFStdUI.exe).
- **Receiver**: *Rx.exe* is the interface to the receiver hardware components. Its purpose is setting up the system, interacting with modules during measurements, performing the necessary signal processing, and to store measurement data. This program is started when measurements are to be performed, given a start-time specified in the user interface (VFStdUI.exe). *MLSW.exe* is the program for interacting with Matlab during measurements, displaying the measurement plots, and is started at the receiver. The user interface program *VFstdUI.exe* is also started at the receiver. All system parameters are stored and defined in parameter files, which can be loaded and adjusted in the

VFstdUI.exe parameter tree view. System parameters encompass all relevant parameters specifying the measurement scenario, such as RF frequency, sampling rate, measurement mode (MIMO, delay-doppler or TIME) and whether averaging of consecutive chirps are to be performed.

- **Network**: Transmitter and Receiver may be connected via Ethernet for synchronization. A program called *VFserver.exe* must be started at the receiver, which acts as a server where the receiver is the master and transmitter is the slave. Anyhow, this requires Ethernet cables, and may introduce timing error. The network connection is therefore omitted. The receiver and transmitter are synchronized (via GPS assisted rubidium clock), and may operate in standalone mode upon an agreed start-time for the measurements.

4.3 Process

The process of performing the measurements were assisted by Odd Trandem at SINTEF, who has been part of the development process of the channel sounder. As in most practical approaches, many obstacles were encountered along the path before the operation of the equipment was satisfying. Once the channel sounder was in place, all components had to be connected in a correct manner. All required components were provided with the channel sounder, except some connector wires, power cords and local oscillators. It is crucial for the local oscillator to be of good quality, i.e. with minimal phase drift, due to the high carrier frequency and long duration of the measurements.

Other problems encountered after setting up the channel sounder were driver problems, inappropriate cables, severe internal loss of signal strength and oscillator phase drift. The original local oscillator at the receiver had to be replaced by a better one, whereas some of the cables initially used introduced an unacceptable signal attenuation at RF frequency. The following error sources had to be corrected before channel measurements were possible:

- The attenuation of channel 1 and 2 of the receiver RF card differed 20dB. Channel 2 had to be used.
- Total cable loss in interconnecting cables was too high. Long cables were replaced by shorter cables, which resulted in a 10dB relative gain overall.
- Local oscillator at receiver: frequency error of 10kHz resulting in phase drift. For a chirp length of 512 samples at $F_s = 100MHz$ (i.e. a chirp duration of 5 microseconds), this frequency error means a 360 degrees phase shift in 100 microseconds. 16 consecutive received chirps are

averaged to produce the estimated channel impulse response, i.e. a phase shift of approximately 290 degrees were experienced during one measurement period. This was corrected by replacing the original local oscillator.

After correcting these error sources and setting the correct Rx and Tx parameters, measurements could be performed. A sketch of the indoor measurement scenario is provided in Figure 4.4.

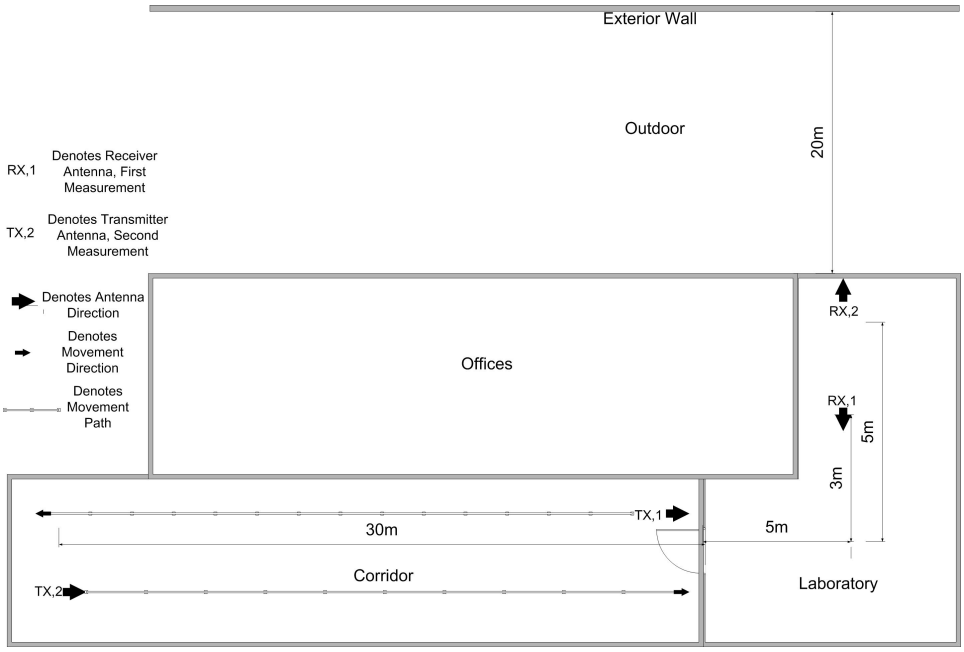

Figure 4.4: Arrangement of Receiver and Transmitter for the 2 indoor channel measurements performed

Two measurement were performed. This first measurement is illustrated in Figure 4.4 with the receiver and transmitter at locations RX,1 and TX,1 respectively, with the antennas angled according to the belonging arrows. The receiver is fixed in the laboratory, whereas the transmitter is moved slowly on a trolley over a distance of 30 meters in approximately 71 seconds. At this speed (0.42 m/s), the Doppler shifts are ignored. The movement is necessary to obtain multiple channel responses.

The second measurement was performed with the transmitter moving the opposite direction. The receiver was rotated 90 degrees and displaced 2 meters. Reflections from the exterior wall outdoor were now also being observed more clearly. The transmitter trolley was shoved along the 30 meters of the corridor in about 63 seconds (0.48 m/s). As with the first measurement, Doppler shifts are ignored.

During both measurements, the varying multipath responses were displayed on the receiver monitor every tenth of a second, and binary data were written to the measurement file. In other words, a measurement duration of 60 seconds would yield approximately 600 channel responses written to disk. Code for reading these stored binary data files is available with the channel sounder software, and can be used to extract channel metrics from the measured data.

4.4 Results and Analysis

The binary datafile written to disk in the measurements can be read and used for estimating the desired RMS delay spread of the channel. As mentioned introductorily, these channel measurements are only valid for this given measurement scenario, i.e. broad conclusions cannot be drawn from these measurements. A plot of the displayed channel impulse responses after about 50 seconds of the first measurement is provided in Figure 4.5, where four distinct signal components can be viewed clearly above the noise floor.

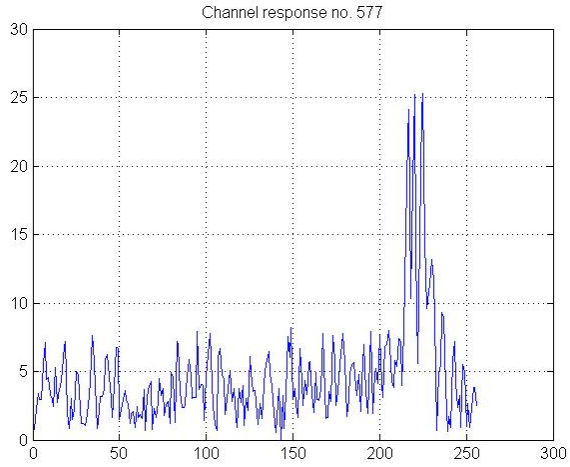

Figure 4.5: Plot of measured channel impulse response of first measurement at t=50s, as a product of averaging of 16 consecutive chirps

The two measurement session of approximately 71 seconds and 63 seconds, generated 706 and 626 measurement records respectively. Each record correspond to one measured channel impulse response, each of which have been produced by averaging of 16 consecutive chirps. All records are written to a measurement file as binary strings. The measurement binary file can be read by the Matlab file "ReadMeas.m" (Appendix A.3.1) which uses the file "TIMEproc.m" (Appendix A.3.2) (The measurement file itself is not included

in this report). These files were provided with the channel sounder software, but are modified to calculate the RMS delay spread of each measured channel according to Equation 2.22. The RMS delay spread is then averaged over the number of measurement records of each measurement session. The estimated RMS delay spread for measurement the first measurement session (71 seconds, 706 records) is displayed in the Matlab console after reading and processing all measurement records:

```
RMS delay spread is: 1.2946e-007=12.9461*Ts
```

Since $F_s = 1/T_s = 100MHz$, the RMS delay spread equals a distance of $12.94 * 3m = 38.82m$, which reflects the indoor scenario described.

The processing of the measurement records of the second measurement session (63 seconds, 626 records) outputs:

```
RMS delay spread is: 1.326e-007=13.26*Ts
```

which equals a distance of $13.26 * 3m = 39.78m$. This also reflects the indoor scenario described.

From Figure 4.5, one might wonder whether a weak received signal component is interpreted as noise or not. The threshold limit used in the RMS delay spread calculation is 10, i.e. amplitude levels exceeding 10 in the impulse response data are interpreted as reflected signal components, whereas levels below 10 are ignored as noise.

Images of the receiver and transmitter equipment is enclosed in Appendix B.0.3 and B.0.4.

Chapter 5

Conclusion

This report has focused on different aspects of multipath fading channels. Theory has been covered, Matlab simulations have been implemented, and channel measurements have been performed. The effects on signal transmission over such time-varying channels have been carefully covered in the theory part, divided in two main focus areas: path-loss and signal fading.

Path loss refers to the mean level of the received signal. The free space path loss describes the loss of a wave traveling some distance. The value of the path-loss cannot be analytically determined in multipath environments, but numerical path-loss models exist for estimating the mean signal level received for various scenarios.

Signal fading, on the other hand, refers the fluctuations in the received signal level about the mean. This fading is either *large-scale* due to shadowing, or *small-scale* as a result of either multipath, Doppler spread or both. Multipath fading causes the channel to be frequency selective, i.e. the channel response is not flat, neither is the phase response linear, over the transmitted signal bandwidth. This introduces increased complexity of the system by means of channel equalization, and the channel frequency response varies as the channel impulse response changes. Doppler effects caused by mobile reception, transmission or scatterers introduces time-dependence to the channel, often modeled as Rayleigh distributed for NLOS environments.

The Matlab simulations illustrate the signal fading effects (small-scale fading), and how a time-variant multipath channel can be measured by a repetitive chirp signal. The capacity of such channels, for both fixed and mobile receiver, was estimated to exceed the capacity of a time-invariant flat channel for a given link budget. The data capacity for WiMAX 256-OFDM transmission was estimated to be 7.35Mbit/s and 7.30Mbit/s given a time-varying multipath channel of 4 paths for mobile and fixed receiver respectively,

whereas a capacity of 5.60Mbit/s was observed for the flat time-invariant channel. This is a result of the increased overall received signal energy due to multiple components, but it also increases the system complexity compared to a flat channel. All capacity simulations are based on a suggested link budget (Table 3.2), providing an outage probability of less than 1%.

The measurements of the time-varying multipath channel impulse response prove that such measurements can be performed in a similar way implemented in the Matlab simulations. The RMS Delay spreads for a moderate number of measurements for two independent indoor measurement sessions (Figure 4.4) ware found to be 1.2946e-007s and 1.326e-007s. This corresponds to a distance spread of 38.82m and 39.78m respectively. This process only states the possibility of extracting channel metrics from practical measurements, and the feasibility of channel measurements.

Chapter 6

Acronyms

AWG Arbitrary Waveform Generator
AWGN Additive White Gaussian Noise
BS Base Station
BW Bandwidth
COST European Cooperation in the Field of Scientific and Technical Research
cPCI Peripheral Component Interconnect
DAC Digital-to-Analog Converter
DFT Discrete Fourier Transform
FFT Fast Fourier Transform
GPIB General Purpose Interface Bus
GPS Global Positioning System
GSM Global System for Mobile Communications
HIPERLAN High Performance Radio Local Area Network
I-channel In-Phase Channel
IFFT Inverse Fast Fourier Transform
ISI Intersymbol Interference
ISM Industrial, Scientific and Medical
LFM Linear Frequency Modulated
LMA Local Mean Attenuation
LOS Line Of Sight
MIMO Multiple Input Multiple Output
MMDS Multipoint Microwave Distribution System
MS Mobile Station
NLOS Non Line Of Sight

Q-channel Quadrature Channel
QoS Quality of Service
RMS Root Mean Square
RX Receiver
SUI Stanford University Interim
TX Transmitter
UMTS Universal Mobile Telecommunications System
WiMAX Worldwide Interoperability for Microwave Access

Appendix A

Code Appendix

A.1 Simulation Code

A.1.1 measurement_simulation.m

```
function measurement_simulation
clear all;
close all;
global_variables_initialize;
NPath = 6; %number of reflected paths
comtype = 2; %1=mobile , 2=fixed
if comtype == 1
[doppler_filter_f doppler_seq_filtered gauss_sequence] = doppler_filter(NPath);
elseif comtype == 2
[doppler_filter_f doppler_seq_filtered gauss_sequence] = gaussian_doppler_filter(NPath);
end
[h g_t h_g_t h_g_t_ideal] = channel_filter_cascade(NPath);
%h=ideal channel response, g_t=raised cosine filter,
%h_g_t=convolution of non-ideal channel response(fraction delay)
%and raised cosine, h_g_t_ideal=convolution of ideal channel
%response and raised cosine.
H_f = fft(h);
H_f_shifted = fftshift(H_f);
s_t = chirp_signal_generation;
s_t_inv = chirp_signal_generation_inverse;
autocorr_chirp = conv(s_t,s_t_inv);
S_t_freq = fft(s_t);
S_t_freq_shifted = fftshift(S_t_freq);
S_t_inv_freq = fft(s_t_inv);
```

```
S_t_inv_freq_shifted = fftshift(S_t_inv_freq);
G_t_freq = fft(g_t);
G_t_freq_shifted = (fftshift(G_t_freq));
[noise_samples noise_level] = generate_noise(0,0,NPath);

figure(1);
global Channel_impulse_response_time_resolution;
global Chirp_Ts;
global Chirp_Fs;
global Channel_impulse_response_freq_resolution;
global Chirp_onesided_BW;
global Chirp_duration;
global H_f_interpol_factor;
t=0:Chirp_Ts:Chirp_duration-Chirp_Ts;
subplot(2,1,1)
stem(t,abs(h))
xlabel('time (0 -> Chirpduration)')
ylabel('channel impulse response')
subplot(2,1,2)
f = -Chirp_Fs/2:(Chirp_Fs/length(H_f)):((Chirp_Fs/2)-(Chirp_Fs/length(H_f)));
plot(f,20*log10(abs(H_f_shifted)));
xlabel(['frequency ( -' num2str(Chirp_Fs/2) '[Hz] ->+' num2str(Chirp_Fs/2) '[Hz] )'])
ylabel('frequency response of H(f) [dB]')

figure(2)
global Chirp_duration;
t = 0:Chirp_Ts:(Chirp_duration-Chirp_Ts);
subplot(2,1,1)
plot(t,real(s_t));
ylabel('amplitude of chirp, real s(t)') %no need plotting imag part

xlabel(['time (0 -> ' num2str(Chirp_duration/Chirp_Ts) '*Ts'])
subplot(2,1,2)
n = -length(autocorr_chirp)/2:1:length(autocorr_chirp)/2-1;
plot(n,(1/(Chirp_duration/Chirp_Ts))*abs(autocorr_chirp));
xlabel('nTs')
ylabel('autocorrelation function |Rss(nTs)|')

figure(3)
f = 0:(Chirp_Fs/length(t)):(Chirp_Fs-(Chirp_Fs/length(t)));
subplot(2,1,1)
plot(f,20*log10((real(S_t_freq_shifted))))
title('Frequency response of chirp')
ylabel('S(f), real [dB]')
```

```
subplot(2,1,2)
plot(f,20*log10(imag(S_t_freq_shifted)))
ylabel('S(f), imag [dB]')
xlabel('frequency')

figure(4)
subplot(2,1,1)
global Approximated_system_filter_onesided_BW;
global system_filter_cutoff_factor;
T = 1/(2*Approximated_system_filter_onesided_BW);
t = -system_filter_cutoff_factor:(2*system_filter_cutoff_factor/length(g_t)):(system_filter_cutoff_factor-
(2*system_filter_cutoff_factor/length(g_t)));
plot(t,g_t);
title('Cos-Roll Off System Filter.')
xlabel(['time. zero-crossings at n*T=n*(1/2*30MHz)'])
ylabel('g(t), square window')
subplot(2,1,2)
f = -Approximated_system_filter_onesided_BW*system_filter_cutoff_factor:
(Approximated_system_filter_onesided_BW*2*system_filter_cutoff_factor/length(G_t_freq_shifted)):
((Approximated_system_filter_onesided_BW*system_filter_cutoff_factor)-
(Approximated_system_filter_onesided_BW*system_filter_cutoff_factor/length(G_t_freq_shifted)));
handler1=plot(f,(abs(G_t_freq_shifted))); hold on;
handler2=stem([-Approximated_system_filter_onesided_BW Approximated_system_filter_onesided_BW]
,[max(abs(G_t_freq_shifted)) max(abs(G_t_freq_shifted))], 'r');
legend([handler1 handler2],['filter response'],['3dB width']);
xlabel(['frequency. One Sided BW=1/2T=30MHz (at 3dB width).'])
ylabel('frequency response |G(f)|')

figure(5);
f = interp((f.*0.5),system_filter_cutoff_factor*2);
t=0:Chirp_Ts:Chirp_duration-Chirp_Ts;
subplot(2,1,1)
plot(t,abs(h_g_t));
title('convolution of raised cosine system filter and channel impulse response (no fading)')
xlabel('time')
ylabel('amplitude')
G_H = fftshift(fft(h_g_t));
subplot(2,1,2)
plot(f,abs(G_H))
title('frequency response of system filter and channel impulse response')
xlabel('baseband frequency')
ylabel('|H(f)*G(f)|')
```

```
figure(6);
global Fast_Fading_Ts_factor;
global Fd;
subplot(3,1,1)
f = -Fd+1:1:Fd-1;
plot(f,abs(doppler_filter_f(1,:)));
title('Doppler spectrum (linear scale) of first tap')
xlabel('doppler frequency');
ylabel('frequency')
subplot(3,1,2)
plot(abs(gauss_sequence(1,:)));
title('gauss sample components (first tap)');
ylabel('abs of real+imag part');
xlabel('sample number')
subplot(3,1,3)
plot(abs(doppler_seq_filtered(1,:)));
title('doppler filtered gauss samples (first tap)')
ylabel('abs of real+imag part');
xlabel('sample number');


%-------------------------
%STARTING SIMULATION CODE.
%-------------------------
%A repetitive chirp signal is sent. Each chirp signal lasts 2048*Ts.
%Ts equals 10ns. 2048*Ts= 20.48microsec. The simulation period is set
%to 100*Chirp_duration=204800*Ts
%The length of the doppler coefficients is 2*Fd*oversampling=8192
%interpolated with Fast_Fading_Ts_factor, i.e. 819200 samples (each of duration Ts). This
means that the first
%100samples of the chirp experiences the same fast fading.

noise_deviation_scale = 0.01; %corresponds to 20dB SNR
noise_samples = noise_samples*noise_deviation_scale; %+ noise_mean;
%scale the noise deviation to fit the scenario described above
figure(7)
stem([1:length(noise_samples)],real(noise_samples));
title('normalized noise samples for chirp signals')
ylabel('amplitude (real part)')
xlabel('noise sample number')

global Measurement_duration;
num_of_chirp_incr = Chirp_duration/Chirp_Ts;
num_of_chirps = (Measurement_duration/Chirp_duration);
```

```
chirp_signals = zeros(1,num_of_chirps*length(s_t));
system_outputs = zeros(1,num_of_chirps*length(s_t));
t = 1;

tau_rms = 0;
global Fast_Fading_Ts_factor;
h_no_doppler = h_g_t;
for k=1:num_of_chirps
tau_avg = 0;
tau_avg_pwr = 0;
h = h_no_doppler;
h_taps = find(abs(h) > (1/log(10+128+1)));
%used for independent fading sequences on each path,
%do not consider sidelobes as seperate paths.
for n=1:length(h_taps)
tap = h(h_taps(n));
%using each coefficient of doppler_seq_filtered for
%Fast_Fading_Ts_factor number of consecutive samples of
%distance Ts
if(n==1) count = 1;
elseif((h_taps(n)-h_taps(n-1))>2) count = count+1;
end
h(h_taps(n))=(doppler_seq_filtered(count,ceil(t/Fast_Fading_Ts_factor))).*tap;
%modifying h according to fast fading

h(h_taps(n))=h(h_taps(n)) + noise_samples(mod((t+n-1),length(noise_samples))+1);
%add independent noise to each path

%coefficients for rms calculation
tau_avg = tau_avg + (tap^2)*(h_taps(n)-h_taps(1));
tau_avg_pwr = tau_avg_pwr + (tap^2)*(h_taps(n)-h_taps(1))^2;
end
tau_rms = tau_rms + (tau_avg_pwr/sum(h(h_taps).^2)) - ((tau_avg/sum(h(h_taps).^2)))^2;


t=t+1;
H_f = fft(h);

%Important: The Simulation Output!
system_outputs(((k-1)*num_of_chirp_incr + 1):(k*num_of_chirp_incr)) =
(1/length(h))*ifft((S_t_freq.*fft(h).*S_t_inv_freq));
end

%tau_rms avaraged over the measurement period
```

```
tau_rms = sqrt(tau_rms/num_of_chirps);
disp(['RMS Delay spread for ' num2str(NPath) ' paths is: ' num2str(abs(tau_rms)) '*Ts (Ts =
10ns)'])

figure(8);
subplot(3,1,1);
plot([1:length(system_outputs(1:num_of_chirp_incr))],fftshift(abs(real(system_outputs(1:num_of_chirp_incr)))));
xlabel('system output with channel and filter, real part (first chirp)')
subplot(3,1,2)
plot([1:length(system_outputs(1:num_of_chirp_incr))],fftshift(abs(imag(system_outputs(1:num_of_chirp_incr)))));
xlabel('system output with channel and filter, imag part (first chirp)')
ylabel('amplitude response (abs)');
subplot(3,1,3)
plot([1:length(system_outputs(1:num_of_chirp_incr))],fftshift(abs((system_outputs(1:num_of_chirp_incr)))));
xlabel('system output with channel and filter, real + imag (first chirp)')


system_output_matrix = zeros(num_of_chirps,num_of_chirp_incr);
for n=1:num_of_chirps
system_output_matrix(n,:) = (system_outputs(((n-1)*num_of_chirp_incr+1):(n*num_of_chirp_incr)));
end
figure(9)
surf((abs((system_output_matrix(:,[1:200])))));
zlabel('amplitude response (abs)')
ylabel('measurement time(chirp number)')
xlabel('local time(n*Ts)')
title('Fast Fading. Reflected Components (absolute value of real+imag) versus Time')


end
```

A.1.2 capacity_simulation.m

```
function capacity_simulation
clear all;
close all;
warning off MATLAB:log:LogOfZero
warning off MATLAB:divideByZero
global_variables_initialize;

channel_type = 1;
%1=mobile, 2=fixed
```

```
NPath = 4; %number of reflected paths
NMeasurement = 1000; %Number of measurements to be simulated
NOFDM = 256;

ignoreFading = 0;
%if ignoreFading=1, the fading is omitted (used for AWGN channel).

OFDM_subcarrier_locations = OFDM_get_subcarriers( NOFDM );
%OFDM symbol with amplitude 1 on datasubcarriers and 2 on pilots.

remove_pilots_indexes = find(OFDM_subcarrier_locations == 2);
OFDM_data_subcarriers_locations = OFDM_subcarrier_locations;

OFDM_data_subcarriers_locations(remove_pilots_indexes) = 0;
%setting pilots to zero for capacity calculations

len = length(OFDM_subcarrier_locations);
Used_frequency_indexes = ((ceil(len/2)-(NOFDM/2)+1):(ceil(len/2)+(NOFDM/2)));

%SNR levels
BPSK_0_5 = 3;
QPSK_0_5 = 6;
QPSK_0_75 = 9;
QAM_16_0_5 = 12;
QAM_16_0_75 = 15;
QAM_64_0_5 = 18;
QAM_64_0_66 = 20;
QAM_64_0_75 = 21;
QAM_64_0_83 = 23;

%Link Budget Parameters
%TRANSMITTER
Transmit_Power_Per_Element = 10; %dBw
Transmit_Antenna_Combination_Gain = 3; %dB, for 2 transmit antennas
Transmit_Antenna_Gain = 12; %dB
Pilot_Power_Boosting_Gain = -0.7;
%dB,loss of pilot power(5/6 of subcarriers used for data)
EIRP = Transmit_Power_Per_Element+Transmit_Antenna_Combination_Gain+
Transmit_Antenna_Gain+Pilot_Power_Boosting_Gain;
disp(' ')
disp('LINK BUDGET PARAMETERS:')
disp(['EIRP=' num2str(EIRP)])
%RECEIVER
```

```
Receiver_Antenna_Gain = 0; %dB, 0 for Mobile, 10 etc for fixed.
Receiver_Antenna_Diversity_Gain = 0; %3dB for 2 antennas (fixed)
Receiver_Noise_Figure = 6;
RECEIVER_GAIN = Receiver_Antenna_Gain+Receiver_Antenna_Diversity_Gain-Receiver_Noise_Figure;
disp(['Receiver Gain=' num2str(RECEIVER_GAIN)])
%NOISE
Noise_Thermal_Density = -194; %dBw/Hz
global Fs_OFDM; %BW of OFDM symbol
TOTAL_TERMAL_NOISE = Noise_Thermal_Density + 10*log10(Fs_OFDM);
%MARGINS
Interference_Margin = 2;
Penetration_Loss = 0; %10 for indoor environments
MARGINS = Interference_Margin+Penetration_Loss;
disp(['Margins=' num2str(MARGINS)])
%PATH LOSS
PATH_LOSS = 140;
disp(['Path Loss=' num2str(PATH_LOSS)])
disp(['Noise=' num2str(TOTAL_TERMAL_NOISE)])

SNR_NO_FADING = (EIRP+RECEIVER_GAIN-MARGINS-PATH_LOSS)-TOTAL_TERMAL_NOISE;
disp(['SNR WITHOUT FADING=' num2str(SNR_NO_FADING)])
disp(['LOWER SNR LIMIT FOR BPSK=' num2str(BPSK_0_5)])
SNR_MARGIN = SNR_NO_FADING - BPSK_0_5;
disp('----------------')
disp(['SNR MARGIN=' num2str(SNR_MARGIN)])
disp('----------------')
%Finished Link Budget parameters. Link budget considered with
%1000 measurements, which then resulted in a BER of 0.88%


H_f_array = zeros(NMeasurement,length(OFDM_subcarrier_locations));
Capacities = zeros(1,NMeasurement);
maxlevels = 0;
maxcapacity = 0;
mincapacity = inf;
minlevels = inf;
sum_Hf = zeros(1,NMeasurement);
SNR_too_low_counter = 0;
[dummy1 doppfilt dummy2] = doppler_filter(1); %used for selecting random fading coeff
[dummy1 gaussdoppfilt dummy2] = gaussian_doppler_filter(1); %used for selecting random fad-
ing coeff

for n=1:NMeasurement
```

```
disp(' ')
disp('***************')
disp(['MEASUREMENT NUMBER:' num2str(n)])
disp('***************')
[h g_t h_g_t h_g_t_ideal] = channel_filter_cascade(NPath);
h = h_g_t;
h_taps = find(abs(h) > (1/log(10+128+1)));
%consider components as distinc paths if amplitude exceeds minimum
%attenuation for a path.
for k=1:length(h_taps)
tap = h(h_taps(k));
if(channel_type==1)
%mobile
if(k==1 || h_taps(k)-h_taps(k-1)>2) %used to distinguish paths from sidelobes
fadingcoeff=doppfilt(ceil(rand*(length(doppfilt))))+j*doppfilt(ceil(rand*(length(doppfilt))));
end
tap = tap*fadingcoeff;
elseif(channel_type == 2)
%fixed
if(k==1 || h_taps(k)-h_taps(k-1)>2) %used to distinguish paths from sidelobes
fadingcoeff=gaussdoppfilt(ceil(rand*(length(gaussdoppfilt))))+j*gaussdoppfilt(ceil(rand*(length(gaussdoppfilt))));
end
tap = tap*fadingcoeff;
end
if(ignoreFading==1)
tap = tap/fadingcoeff;
end
h(h_taps(k))=tap;
%update according to fading
end

H_f_array(n,:) = fftshift(fft(h,length(OFDM_subcarrier_locations)));
sum_Hf(n) = sum(H_f_array(n,:));

received_levels=20*log10(abs(H_f_array(n,:).*OFDM_data_subcarriers_locations));

receivedSNR = zeros(length(Used_frequency_indexes));
Capacity = 0;

k=1;
subclength = length(OFDM_subcarrier_locations);
for l=((ceil(subclength/2)-(NOFDM/2)+1):(ceil(subclength/2)+(NOFDM/2)))
receivedSNR(k) = received_levels(l)+SNR_NO_FADING;
```

```
if (BPSK_0_5<=receivedSNR(k) && receivedSNR(k)<QPSK_0_5)
Capacity = Capacity + 1*0.5;
%capacity of subcarrier n with BPSK 1/2 rate
elseif (QPSK_0_5<=receivedSNR(k) && receivedSNR(k)<QPSK_0_75)
Capacity = Capacity + 2*0.5;
%capacity of subcarrier n with QPSK 1/2 rate
elseif (QPSK_0_75<=receivedSNR(k) && receivedSNR(k)<QAM_16_0_5)
Capacity = Capacity + 2*0.75;
%capacity of subcarrier n with QPSK 3/4 rate
elseif (QAM_16_0_5<=receivedSNR(k) && receivedSNR(k)<QAM_16_0_75)
Capacity = Capacity + 4*0.5;
%capacity of subcarrier n with 16QAM 1/2 rate
elseif (QAM_16_0_75<=receivedSNR(k) && receivedSNR(k)<QAM_64_0_5)
Capacity = Capacity + 4*0.75;
%capacity of subcarrier n with 16QAM 3/4 rate
elseif (QAM_64_0_5<=receivedSNR(k) && receivedSNR(k)<QAM_64_0_66)
Capacity = Capacity + 6*0.5;
%capacity of subcarrier n with 64QAM 1/2 rate
elseif (QAM_64_0_66<=receivedSNR(k) && receivedSNR(k)<QAM_64_0_75)
Capacity = Capacity + 6*(2/3);
%capacity of subcarrier n with 64QAM 2/3 rate
elseif (QAM_64_0_75<=receivedSNR(k) && receivedSNR(k)<QAM_64_0_83)
Capacity = Capacity + 6*(3/4);
%capacity of subcarrier n with 64QAM 3/4 rate
elseif (QAM_64_0_83<=receivedSNR(k))
Capacity = Capacity + 6*(5/6);
%capacity of subcarrier n with 64QAM 5/6 rate
else
Capacity = Capacity + 0; %too low SNR
if(OFDM_data_subcarriers_locations(l)>0)
SNR_too_low_counter = SNR_too_low_counter + 1;
%only data carriers considered
end
end
k = k+1;
end


Symbol_duration = 102.9*10^-6;
Capacities(1,n) = Capacity/Symbol_duration;

if (Capacities(1,n)>maxcapacity)
maxlevels = received_levels+SNR_NO_FADING;
maxcapacity = Capacities(1,n);
```

```
end
if (Capacities(1,n)<mincapacity)
minlevels = received_levels+SNR_NO_FADING;
mincapacity = Capacities(1,n);
end

end


figure(1);
subplot(3,1,1);
f = [((-1/2):(1/length(H_f_array(NMeasurement,:))):((1/2)-1/length(H_f_array(NMeasurement,:))))];
plot(f,20*log10(abs(H_f_array(NMeasurement,:))))
title('Response of channel and system filter cascade last measurement')
ylabel('Frequency Response [dB]')
xlabel('Frequencies. -50MHz -> +50MHz')
subplot(3,1,2);
index = ((ceil(len/2)-(NOFDM/2)+1):(ceil(len/2)+(NOFDM/2)));
stem(OFDM_subcarrier_locations(index));
title('transmitted ofdm symbol (simplified) for capacity estimations')
xlabel('subcarrier number')
ylabel('amplitude')
subplot(3,1,3)
stem(received_levels(index))
global Fs_OFDM;
title(['Response of channel and system filter cascade at last measurement over OFDM BW='
num2str(Fs_OFDM)])
xlabel('subcarrier number')
ylabel('level [dB]')

figure(2);
subplot(2,1,1)
stem(maxlevels(index))
title(['received levels at maximum capacity of:' num2str(floor(maxcapacity)) 'bits/sec'])
ylabel('amplitude [dB]')
xlabel('subcarrier number')
subplot(2,1,2)
stem(minlevels(index))
title(['received levels at minimum capacity of:' num2str(floor(mincapacity)) 'bits/sec'])
ylabel('amplitude [dB]')
xlabel('subcarrier number')

global data_carriers;
disp(' ')
```

```
disp('CAPACITY METRICS:')
avg = mean(Capacities);
sigma = std(Capacities);
disp(['Mean value:' num2str(avg) 'bit/s']);
disp(['Standard deviation:' num2str(sigma) 'bit/s']);
disp(['Maximum measured capacity:' num2str(maxcapacity) 'bit/s']);
disp(['Minimum measured capacity:' num2str(mincapacity) 'bit/s']);
disp(['Maximum theoretical capacity(QAM64 5/6 rate over all carriers):' num2str(data_carriers*6*(5/6)/Symbol_duration)
'bit/s'])
disp(' ');

figure(3);
cap_min = min(Capacities);
cap_max = max(Capacities);
range = cap_min:(cap_max-cap_min)/(length(Capacities)-1):cap_max;
cap_sorted = sort(Capacities);
cap_cdf = zeros(1,length(range));
for n=1:length(range)
cap_cdf(n) = length(find(cap_sorted<range(n)));
end
cap_cdf = cap_cdf./length(cap_cdf);
plot(range,cap_cdf)
title('Empirical Capacity CDF')
xlabel('Capacity (bit/s)')
ylabel('Probability P(c<=C)')
%subplot(2,1,2)
figure(4);
hist(Capacities,20);
title(['Capacity histogram of ' num2str(NMeasurement) ' Measurements'])
xlabel('Capacity bins (bit/s)')
ylabel('Number of occurences')

figure(5)
cdfplot(Capacities);

range_subcarriers=[((ceil(subclength/2)-(NOFDM/2)+1):(ceil(subclength/2)+(NOFDM/2)))];
SNR_too_low_data_carriers_avg = SNR_too_low_counter/NMeasurement;
num_of_data_carriers = length(find(OFDM_data_subcarriers_locations>0));
disp(['Number of data carriers:' num2str(num_of_data_carriers)])
disp(['Number of data carriers below 3dB averaged over ' num2str(NMeasurement) ' measure-
ments is:' num2str(SNR_too_low_data_carriers_avg)])
disp(['This gives an outage probability of ' num2str(SNR_too_low_data_carriers_avg*100/num_of_data_carriers)
'%'])
```

```
end
```

A.2 Base Code

A.2.1 global_variables_initialize.m

```
function global_variables_initialize

global c;
global Fs;
global Fc;
global Fd;
global Gauss_Oversampling_factor;
global Fast_Fading_Ts_factor;
global Channel_impulse_response_time_resolution;
global Channel_impulse_response_freq_resolution;
global Chirp_onesided_BW;
global Chirp_Fs;
global Chirp_oversampling_factor;
global Chirp_Ts;
global Chirp_duration;
global H_f_interpol_factor;
global Approximated_system_filter_onesided_BW;
global Approximated_system_filter_oversampling_factor;
global Approximated_system_filter_rolloff;
global system_filter_cutoff_factor;
global Wavelength;
global Measurement_duration;
global Fs_OFDM;
global data_carriers;
Fs_OFDM = 0; %to be set in OFDM_get_data_subcarriers
data_carriers = 0; %to be set in OFDM_get_data_subcarriers

c = 3*(10^8); %Speed of light
Fc = 2100000000; %Carrier frequency
Gauss_Oversampling_factor = 64; %Oversampling factor for the gauss
%sequence input to the doppler filter
Fd = 50; %doppler filter one sided BW
Fast_Fading_Ts_factor = 1; %means grade of interpolation used for the
%fading coefficients. 1 means no interpolation.
Channel_impulse_response_time_resolution = 100;
Channel_impulse_response_freq_resolution = 100;
```

```
Chirp_onesided_BW = 20000000; %One-sided bandwidth of chirp signal
Chirp_Fs = 100000000; %Sample frequency of chirp signal
Chirp_oversampling_factor = Chirp_Fs/(2*Chirp_onesided_BW); %Oversampling of chirp sig-
nal (5/2)
Chirp_Ts = 1/Chirp_Fs; %Sample duration. 10ns = 3m.
Chirp_duration = 2048*Chirp_Ts; %time-span for chirp to change from -20MHz to +20MHz

H_f_interpol_factor = 50; %number of interpolations between consecutive Ts in H_f

Approximated_system_filter_onesided_BW = 30000000; %DAC-filter, smoothing-filter and an-
tialiasing
%filter can be approximated with a cos-roll-off
%filter with onesided BW of 30MHz
Approximated_system_filter_oversampling_factor = Chirp_Fs/(2*Approximated_system_filter_onesided_BW);
%Overampling factor of system_filter
Approximated_system_filter_rolloff = 0.5; %Roll-off factor of raised-cosine filter

system_filter_cutoff_factor = 8; %cutoff raised cosine filter at +/- 8*Ts

Wavelength = c/Fc; %14,3 cm at 2,1GHz
Measurement_duration = 100*Chirp_duration; %Duration for measurement simulation

end
```

A.2.2 chirp_signal_generation.m

```
function s_t = chirp_signal_generation

global Chirp_Ts;
global Chirp_onesided_BW;
global Chirp_duration;
num_of_increments = Chirp_duration/Chirp_Ts; %1024 or 2048 increments.
t = 0:Chirp_Ts:(Chirp_duration-Chirp_Ts);
s_t_real = chirp(t,-Chirp_onesided_BW,Chirp_Ts*num_of_increments/2,0);
%cosine part, starting at t=0,F=-Chirp_onesided_BW
%passing F=0 at length(t)/2
s_t_imag = (chirp(t,-Chirp_onesided_BW,Chirp_Ts*num_of_increments/2,0,'linear',90)).*j;
%sine part, equals cosine shifted 90 degrees
s_t = s_t_real + s_t_imag;

end
```

A.2.3 chirp_signal_generation_inverse.m

```
function s_t = chirp_signal_generation_inverse

global Chirp_Ts;
global Chirp_onesided_BW;
global Chirp_duration;
num_of_increments = Chirp_duration/Chirp_Ts; %1024 or 2048 increments.
t = 0:Chirp_Ts:(Chirp_duration-Chirp_Ts);
s_t_real = chirp(t,-Chirp_onesided_BW,Chirp_Ts*num_of_increments/2,0);
%cosine part, starting at t=0,F=-Chirp_onesided_BW
%passing F=0 at length(t)/2
s_t_imag = (chirp(t,-Chirp_onesided_BW,Chirp_Ts*num_of_increments/2,0,'linear',90)).*j;
%sine part, equals cosine shifted 90 degrees
s_t = s_t_real - s_t_imag;

end
```

A.2.4 channel_filter_cascade.m

```
function [h_t_ideal g_t h_g_t h_g_t_ideal] = channel_filter_cascade(NPath)
global Fc;
global Chirp_Ts;
global Chirp_duration;
global H_f_interpol_factor;
global Chirp_oversampling_factor;
oversampling = Chirp_oversampling_factor;
resolution = Chirp_Ts;
duration = Chirp_duration;
num_of_chirp_increments = duration/resolution;

%-------------------------------
%STARTING WITH THE CHANNEL IMPULSE RESPONSE: h(t)
%-------------------------------
%the delays are given in relative format, i.e. delay =
%relative delay. The relative delay of the first arriving component is zero
relative_delays = zeros(1,NPath);
disp(' ')
disp('DELAY RELATIVE TO duration:')
disp([' relative delay of the first arriving component is 0'])
for n=2:NPath
relative_delays(n) = (1/num_of_chirp_increments)*
```

```
(min(((abs(rand)*num_of_chirp_increments/16)+1),(num_of_chirp_increments/16)));
%delay between 1 and num_of_chirp_increments/16 for chirp durations of 1024/2048 Ts
%delay of 1=3m path difference, while 64=192m path difference. OK for
%indoor short range measurements.
end

relative_delays = sort(relative_delays);
for n=2:NPath
disp([' relative delay of reflected component ' num2str(n) ' is ' num2str(relative_delays(n))]);
end
disp(' ')

%the phase differences of the reflected components are relative to the
%first arriving component. The phase is uniformly distributed in [0,2*pi]
relative_phase_diff = zeros(1,NPath);
disp('RELATIVE PHASE DIFFERENCE OF FIRST AND SUBSEQUENT REFLECTED COM-
PONENTS:')
disp([' phase of the first arriving component is 0'])
for n=2:NPath
relative_phase_diff(n) = rand*2*pi;%(round(rand*10))*2*pi/10;
disp([' phase of reflected component ' num2str(n) ' is ' num2str(relative_phase_diff(n))])
end
disp(' ')


a = ones(1,NPath);
disp('RELATIVE ATTENUATION:')
disp([' relative attenuation, a0, of the first arriving component is ' num2str(a(1))])

for n=2:NPath
a(n) = 1/(log10((10+num_of_chirp_increments*(relative_delays(n)))));
%log-normal shadowing and path loss only. Fading is included in
%simualtions.
end
a = sort(a,'descend');
for n=2:NPath
disp([' attenuation of reflected component ' num2str(n) ' is ' num2str(a(n))])
end

global Channel_impulse_response_time_resolution;
global Chirp_onesided_BW;
global Fc;
global Chirp_Fs;
```

```
h_g = zeros(1,num_of_chirp_increments); %for arbitrary delays.. convolution of h and g resampled
%this is used for simulation where fraction delays are allowed
h_g_ideal = zeros(1,num_of_chirp_increments); %for delays of order n*Chirp_Ts (ideal delays)

h_ideal = zeros(1,num_of_chirp_increments); %ideal delay impulse response, used for illustration purposes.
freq_resolution = Chirp_duration/Chirp_Ts; %Chirp_Fs/1000000;
H = zeros(1,freq_resolution);



temp = zeros(1,NPath);
n=1;
f_lo = -(Chirp_Fs/2)/1000000;
f_hi = (Chirp_Fs/2)/1000000;
f = f_lo;
freq_incr = (f_hi-f_lo)/freq_resolution;
global Approximated_system_filter_onesided_BW;
Ts = 1/Approximated_system_filter_onesided_BW;
for t=0:resolution:duration-resolution
for k=1:NPath
%h_g and h_g_ideal: convolution of system filter (cos roll off)
%and channel impulse response. "ideal" means only integer
%number of Ts delay in channel impulse response, whereas h_g
%includes arbitrary delay. The term "0*relative_delays(k)" is due to
%baseband considerations.
h_g(n) = h_g(n)+(a(k)/a(1))*cos_roll_off(t-4*Ts-relative_delays(k)*duration)*exp(j*(relative_phase_diff(k)-0*relative_delays(k)*duration));
h_g_ideal(n) = h_g_ideal(n)+
(a(k)/a(1))*cos_roll_off(t-4*Ts-(ceil(relative_delays(k)*num_of_chirp_increments)/num_of_chirp_increments)*duration)
*exp(j*(relative_phase_diff(k)-0*relative_delays(k)*duration));
h_ideal(n) = h_ideal(n)+
(a(k)/a(1))*dirac_discrete(t-(ceil(relative_delays(k)*num_of_chirp_increments)/num_of_chirp_increments)*duration)
*exp(j*(relative_phase_diff(k)-0*relative_delays(k)*duration));
end
n=n+1;
end

n=1;
global system_filter_cutoff_factor;
for t = -system_filter_cutoff_factor*Ts:(Ts/system_filter_cutoff_factor):(system_filter_cutoff_factor*Ts-(Ts/system_filter_cutoff_factor))
```

```
g(n) = cos_roll_off(t);
n=n+1;
end

g_t = g;
h_t_ideal = h_ideal;
h_g_t = h_g;
h_g_t_ideal = h_g_ideal;
end
```

A.2.5 cos_roll_off.m

```
function val = cos_roll_off(t)

global Chirp_Ts;
global Approximated_system_filter_onesided_BW;
global Approximated_system_filter_rolloff;
beta = Approximated_system_filter_rolloff;
Ts = 1/Approximated_system_filter_onesided_BW;
val1 = cos(pi*beta*t/Ts);
val2 = (1 - (4*(beta^2)*(t^2)/(Ts^2)));
if (val1==val2)
val = sinc(t/Ts);
else
val = sinc(t/Ts)*(val1/val2);
end

end
```

A.2.6 doppler_filter.m

```
function [doppler_filter gauss_filtered gauss_sequence] = doppler_filter(NPath)

%Doppler_filter calculates doppler coefficients for the N Paths
%NPath is the number of paths in the multipath environment

global Fd; %max doppler shift (doppler frequency)
global Chirp_Ts;
global Fast_Fading_Ts_factor;
%end values omitted
%due to infinite-valued
```

```
%doppler spectrum.
Sd = zeros(NPath,length(f));
for k=1:NPath
for i=1:1:length(f)
Sd(k,i) = (1/4*pi*Fd)*(1/sqrt(1-(f(i)^2)/(Fd^2))); %doppler spectrum
end
end
Doppler_BW = 2*Fd;
global Gauss_Oversampling_factor;
%gauss symbol should have large oversampling factor compared to
%the Doppler_BW, i.e. a long sequence of correlated gauss samples
%are produced in the filtering process.
gauss_sekv_BW = Doppler_BW*Gauss_Oversampling_factor;
gauss_sekv_duration = 1/gauss_sekv_BW;
Sd1 = zeros(NPath,gauss_sekv_BW);
gauss_re = randn(NPath,gauss_sekv_BW); %create vector of complex gaussian values, real part.

gauss_im = randn(NPath,gauss_sekv_BW); %create vector of complex gaussian values, imaginary part.
avg = zeros(1,NPath);
f = 1:gauss_sekv_BW;
for k=1:NPath
for n=1:(length(Sd(k,:)))
Sd1(k,((length(Sd1(k,:))/2)-Fd)+n) = Sd(k,n);
end
gauss_freq(k,:) = (1/Gauss_Oversampling_factor)*fft((gauss_re(k,:)+j*gauss_im(k,:)),gauss_sekv_BW);
Gauss_Filt(k,:) = gauss_freq(k,:).*Sd1(k,:);
Gauss_Filt_time_domain(k,:) = ifft(Gauss_Filt(k,:));
avg(k) = sum(abs(Gauss_Filt_time_domain(k,:)))/length(Gauss_Filt_time_domain(k,:));
%used for normalizing output (i.e. average amplitude of 1 is preferred)
end
t = 0:(length(Sd1(1,:))-1);

%the avarage amplitude values of Gauss_filt_time_domain must equal 1.
%i.e. the scale factor on the taps must produce an output with avarage
%amplitud value of unity.
for k=1:NPath
Gauss_Filt_time_domain(k,:) = Gauss_Filt_time_domain(k,:)./avg(k);
end

doppler_filter = Sd;
gauss_filtered = Gauss_Filt_time_domain;
gauss_sequence = gauss_re + j.*gauss_im;
```

```
end
```

A.2.7 gaussian_doppler_filter.m

```
function [doppler_filter gauss_filtered gauss_sequence] = gaussian_doppler_filter(NPath)
%gaussian_doppler_filter calculates doppler coefficients for the N Paths in
%a fixed "mobile" communication environment, i.e. only the reflectors are moving.
%NPath is the number of paths in the multipath environment

global Fd; %max doppler shift (doppler frequency)
global Chirp_Ts;
global Fast_Fading_Ts_factor;

end values omitted
%due to infinite-valued doppler spectrum.

Sd = zeros(NPath,length(f));
sigma = Fd/3; %cutoff at 3*sigma
for k=1:NPath
for i=1:1:length(f)
Sd(k,i) = exp(-((i-Fd)^2)/(2*(sigma^2))); %gaussian doppler spectrum
end
end

Doppler_BW = 2*Fd;
global Gauss_Oversampling_factor;
%gauss symbol should have large oversampling factor compared to
%the Doppler_BW, i.e. a long sequence of correlated gauss samples
%are produced in the filtering process.
gauss_sekv_BW = Doppler_BW*Gauss_Oversampling_factor;
gauss_sekv_duration = 1/gauss_sekv_BW;

Sd1 = zeros(NPath,gauss_sekv_BW);
gauss_re = randn(NPath,gauss_sekv_BW); %create vector of complex gaussian values, real part.

gauss_im = randn(NPath,gauss_sekv_BW); %create vector of complex gaussian values, imaginary part.
avg = zeros(1,NPath);
f = 1:gauss_sekv_BW;
for k=1:NPath
for n=1:(length(Sd(k,:)))
Sd1(k,((length(Sd1(k,:))/2)-Fd)+n) = Sd(k,n);
```

```
end
gauss_freq(k,:) = (1/Gauss_Oversampling_factor)*fft((gauss_re(k,:)+j*gauss_im(k,:)), gauss_sekv_BW);
Gauss_Filt(k,:) = gauss_freq(k,:).*Sd1(k,:);
Gauss_Filt_time_domain(k,:) = ifft(Gauss_Filt(k,:));
avg(k) = sum(abs(Gauss_Filt_time_domain(k,:)))/length(Gauss_Filt_time_domain(k,:));
end
t = 0:(length(Sd1(1,:))-1);

%the avarage amplitude values of Gauss_filt_time_domain must equal 1.
%i.e. the scale factor on the taps must produce an output with avarage
%amplitud value of unity.
for k=1:NPath
Gauss_Filt_time_domain(k,:) = Gauss_Filt_time_domain(k,:)./avg(k);
end
doppler_filter = Sd;
gauss_filtered = Gauss_Filt_time_domain;
gauss_sequence = gauss_re + j.*gauss_im;

end
```

A.2.8 generate_noise.m

```
function [noise_Ts_samples noise_Ts_samples_level] = generate_noise(noise_level, noise_factor,
NPath)
%thermal noise and receiver noise.
%noise_factor: noise factor in dB at receiver front end, typically caused by LNA.
%noise_level: suggested noise level in dBm/Hz (default: -174)
if(noise_level == 0)
noise_level = -174;
end
if(noise_factor == 0)
noise_factor = 7;
end
global Chirp_Fs;
global Chirp_Ts;
global Measurement_duration;
global Chirp_duration;
num_of_measurements = Measurement_duration/Chirp_duration;
noise_BW = Chirp_Fs;
thermal_noise_power_dB = noise_level + 10*log10(noise_BW);
%if noise_level=-174, Fs=100MHz -> -94dBm = 3.98*10^-10mW
thermal_noise_power = 10^(thermal_noise_power_dB/10);
```

```
total_noise_power_dB = thermal_noise_power_dB + noise_factor;
total_noise_power = 10^(total_noise_power_dB/10);

noise_samples = randn(1,num_of_measurements*NPath)+j*randn(1,num_of_measurements*NPath);

noise_Ts_samples = noise_samples;
noise_Ts_samples_level = total_noise_power;

end
```

A.2.9 OFDM_get_subcarriers.m

```
function subcarriers_return = OFDM_get_data_subcarriers( NOFDM )
%"dummy" function for retrieving the carriers of OFDM used for capacity
%estimations. Only the frequency location and BW of the OFDM symbol
%is of interest, i.e. no real data is needed to estimate the capacity,
%so this is only a very superficial OFDM symbol.
%NOFDM must equal 512 or 1024, focusing on 802.16e (mobile) downlink
global Chirp_Fs;
global Chirp_Ts;
global Chirp_duration;
Num_of_channel_samples = Chirp_duration/Chirp_Ts;
channel_samples_freq_spacing = Chirp_Fs/(Num_of_channel_samples-1);
OFDM_freq_spacing = 10940; %Hz
global Fs_OFDM;
Fs_OFDM = round(OFDM_freq_spacing*NOFDM*10)/10;
New_Num_of_channel_samples = round(Chirp_Fs/OFDM_freq_spacing);
%used for returning an array of subcarriers at the correct
%frequency locations according the the existing channel
%frequency response.
subcarriers = zeros(1,New_Num_of_channel_samples);
mid_index = ceil(length(subcarriers)/2);
global data_carriers;
if NOFDM==512
data_carriers = 360;
pilot_carriers = 60;
null_carriers = 92;
elseif NOFDM==1024
data_carriers = 720;
pilot_carriers = 120;
null_carriers = 184;
```

```
elseif NOFDM==256
data_carriers = 192;
pilot_carriers = 8;
null_carriers = 56;
end


for n = (mid_index-(NOFDM/2)+1):1:(mid_index+NOFDM/2)
k = n-(mid_index-(NOFDM/2));
if(k<=((null_carriers/2)-1) || k>(NOFDM-null_carriers/2) || n==mid_index)
%do nothing..null carriers
else if(mod((k-1),(data_carriers/pilot_carriers))==0)
subcarriers(n) = 2; %pilot carriers, no data
else
subcarriers(n) = 1; %data carrier!
end
end
end

subcarriers_return = subcarriers;

end
```

A.3 Channel Measurement Data Acquisition Code

A.3.1 ReadMeas.m

```
 % ReadMeas.m
%Measurement number 1 filepath:
path1='KorridorTst1_tid_65.mes';

%Measurement number 2 filepath:
path2='KorridorTst2_tid_55.mes';

filename = path1;

fid=fopen(filename,'r');


% 'float64' 'int16'

%
```

```
% Read description section (text)
%

dstr=zeros(8,1);
ENDOFDESC=[hex2dec('12') hex2dec('34') hex2dec('56') hex2dec('78') hex2dec('89') hex2dec('ab')
hex2dec('cd') hex2dec('ef')]';
i=1;
while i<144&sum(abs(dstr-ENDOFDESC)) =0
dstr=fread(fid,8,'uchar');
if i==1
str=char(dstr');
i=2;
else
str = [str char(dstr')];
i=i+1;
end
end
disp(str(1:length(str)-8));

NoRecords = fread(fid,1,'int32')
MeasMode = fread(fid,1,'int32')
TAVEKk = fread(fid,1,'int32')
RecDescSize = fread(fid,1,'int32')

n=0;
n=n+1; Nchannels = fread(fid,1,'int32') % Number of channels (1 or 2)
n=n+1; Nch = fread(fid,1,'int32') % Number of complex samples per chirp (decimated)
n=n+1; Nav = fread(fid,1,'int32') % Number of chirps to average
n=n+1; Naw = fread(fid,1,'int32') % Number of chirps to average written in file
n=n+1; Nrxant = fread(fid,1,'int32') % Number of antennas at transmitter
n=n+1; Ntxant = fread(fid,1,'int32') % Number of antennas at receiver
n=n+1; Ndopp = fread(fid,1,'int32') % Number of doppler channels
n=n+1; ChBetwBurst = fread(fid,1,'int32') % Number of chirps between each acquisition burst
n=n+1; ChBetwMeas = fread(fid,1,'int32') % Number of chirps between each measurement
n=n+1; align = fread(fid,1,'int32'); % to align only
n=n+2; Fs = fread(fid,1,'double') % Decimated sample rate
n=n+2; ChBandw = fread(fid,1,'double') % Chirp bandwidth in
n=n+1; RecordHeadSize = fread(fid,1,'int32') % Size of record header in bytes
n=n+1; RecordDataSize = fread(fid,1,'int32') % Size of each record data section in bytes


if 4*n =RecDescSize
fclose(fid);
error('RecDescSize not equal to size of record descriptor');
```

```
end


%
% Read records
%
Channel = zeros(1,NoRecords);
Hour = zeros(1,NoRecords);
Min = zeros(1,NoRecords);
Second = zeros(1,NoRecords);
Millisec = zeros(1,NoRecords);
fTime = zeros(1,NoRecords);
fTxLong = zeros(1,NoRecords);
fTxLat = zeros(1,NoRecords);
fRxLong = zeros(1,NoRecords);
fRxLat = zeros(1,NoRecords);
fRxLevel = zeros(1,NoRecords);
fDataScale = zeros(1,NoRecords);

% Make referance chirp
global SampFreqDec
global ChirpBandw
global NchirpDec
SampFreqDec = Fs
ChirpBandw = ChBandw;
NchirpDec = Nch;

global recn

MakeRefChirp;

Lrec = RecordDataSize/4;

% Read and process each record
global NoRecords;
global counter;
global RMSdelspread;
RMSdelspread = 0;
counter = 0;
NoRecords
for recn=1:NoRecords
Channel(recn) = fread(fid,1,'int32'); % 1 or 2 = channel number
Hour(recn) = fread(fid,1,'int16'); % Time on format hour:minute:second:millisecond, as 4 16 bit
integers
```

```
Min(recn) = fread(fid,1,'int16');
Second(recn) = fread(fid,1,'int16');
Millisec(recn) = fread(fid,1,'int16');
fTime(recn) = fread(fid,1,'float32'); % Time on format float second since 00:00:00 midnight
fTxLong(recn) = fread(fid,1,'float32'); % Tx Longitude - degrees with decimals - 32 bit float
fTxLat(recn) = fread(fid,1,'float32'); % Tx Latitude - degrees with decimals - 32 bit float
fRxLong(recn) = fread(fid,1,'float32'); % Rx Longitude - degrees with decimals - 32 bit float
fRxLat(recn) = fread(fid,1,'float32'); % Rx Latitude - degrees with decimals - 32 bit float
fRxLevel(recn) = fread(fid,1,'float32'); % RMS data level dBm - 32 bits float
fDataScale(recn) = fread(fid,1,'float32'); % Scale factor, Multiply data by this, and get antenna
voltage in mV (float)


reca = fread(fid,2*Lrec,'int16');
Rec = (reca(1:2:2*Lrec-1) + sqrt(-1)*reca(2:2:2*Lrec)) / 32768;

if Naw =1
error ('Processing currently only implemented for Naw = 1!');
fclose(fid);
end

if MeasMode==1
TIMEproc(recn,Rec,0);
pause(0.2);
elseif MeasMode==5
DelDop (Rec, NchirpDec, Ndopp);title(['Rec no. ' num2str(recn)]);
pause(0.4);
else % DOA TDOA DDOA
DelDop (Rec, NchirpDec, Nrxant*Ntxant);title(['Rec no. ' num2str(recn)]);
pause(0.4);
end
end

fclose(fid);
```

A.3.2 TIMEproc.m

```
function TIMEproc(recn, Rec, init)

global RefChirp;
global RMSdelspread;
global NoRecords;
```

```
global counter;
lrec = length(Rec);

C=fft(Rec.');
H=C.*RefChirp;
h=ifft(H);
i=0;
firstcomp=0;
for n=1:length(h)
if(abs(h(n))>10)
i=i+1;
if(i==1)
comp(i)=abs(h(n));
delay(i)=0;
firstcomp=n;
else
comp(i)=abs(h(n));
delay(i)=(n-firstcomp)*(1/100000000);
end
end
end
tauavg = (sum((comp.^2).*delay))/sum(comp.^2);
tauavgpwr = (sum((comp.^2).*(delay.^2)))/sum(comp.^2);
RMSdelspread = RMSdelspread + (sqrt(tauavgpwr-tauavg^2))/NoRecords;
counter = counter + 1;
if(counter==NoRecords)
disp(['RMS delay spread is: ' num2str(RMSdelspread) '=' num2str(RMSdelspread*100000000)
'*Ts'])
end

alh=fftshift((abs(h)));
figure(2);plot(abs(alh));grid;
title(['Channel response no. ' num2str(recn)]);
```

Appendix B

Figure Appendix

B.0.3 Channel Measurements: Receiver Rack

Figure B.1: Receiver Equipment

B.0.4 Channel Measurements: Transmitter Rack

Figure B.2: Transmitter Equipment

Bibliography

[1] Andrea Goldsmith. *Wireless Communications*, pages 42–44. Cambridge University Press, 2005.

[2] Theodore S. Rappaport. *Wireless Communications - Principles and Practice*, page 152. Prentice Hall, second edition, 2002.

[3] Gordon L. Stüber. *Principles of Mobile Communication*, page 109. Kluwer Academic Publishers, second edition, 2001.

[4] AG Burr. Wide-band channel modelling using a spatial model. *Spread Spectrum Techniques and Applications, 1998. Proceedings., 1998 IEEE 5th International Symposium on*, 1, 1998.

[5] Andrea Goldsmith. *Wireless Communications*, page 48. Cambridge University Press, 2005.

[6] Theodore S. Rappaport. *Wireless Communications - Principles and Practice*, page 208. Prentice Hall, second edition, 2002.

[7] B. Sklar. Rayleigh fading channels in mobile digital communication systems. i. characterization. *Communications Magazine, IEEE*, 35(7):90–100, 1997.

[8] F. Ling. Matched filter-bound for time-discrete multipath Rayleigh fadingchannels. *Communications, IEEE Transactions on*, 43(234):710–713, 1995.

[9] RB Ertel and JH Reed. Generation of two equal power correlated Rayleigh fading envelopes. *Communications Letters, IEEE*, 2(10):276–278, 1998.

[10] A. Abdi, C. Tepedelenlioglu, M. Kaveh, and G. Giannakis. On the estimation of the K parameter for the Rice fadingdistribution. *Communications Letters, IEEE*, 5(3):92–94, 2001.

[11] Amit Aggarwal and Erlend Hansen. link: http://cnx.org/content/m11718/latest/, Apr 24, 2007.

[12] RM Narayanan and M. Dawood. Doppler estimation using a coherent ultrawide-band random noiseradar. *Antennas and Propagation, IEEE Transactions on*, 48(6):868–878, 2000.

[13] Gregory D. Durgin. Wireless communications: Modeling random fading channels, from the book: Space-time wireless channels (prentice hall), link: http://www.phptr.com/articles/article.asp?p=169488&seqnum=4&rl=1, Mar 5, 2004.

[14] IEEE. *802.16-2004 Part 16: Air Interface for Fixed Broadband Wireless Access Systems*, OCT 1, 2004.

[15] WiMAX-Forum. Mobile WiMAX - Part I: A Technical Overview and Performance Evaluation, 2006.